Supplementary Information for

Spatial confinement and temporal dynamics of selectin ligands enable stable hematopoietic stem cell rolling

Bader Al Alwan[1‡], Karmen AbuZineh[1], Shuho Nozue[1], Aigerim Rakhmatulina[1], Mansour Aldehaiman[1], Asma S. Al-Amoodi[1], Maged F. Serag[1], Fajr A. Aleisa[1], Jasmeen S. Merzaban[1†] and Satoshi Habuchi[1†]**

[1] King Abdullah University of Science and Technology (KAUST), Biological and Environmental Science and Engineering Division, Thuwal 23955-6900, Saudi Arabia

Contents

Supplementary Figures

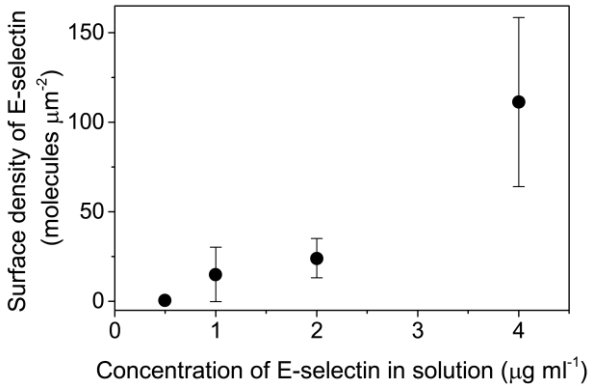

Supplementary Figure 1. Surface density of rh E-selectin molecules. The surface densities of the rh E-selectin molecules were determined after incubating the microfluidic chambers with HBSS buffer containing different concentrations of the recombinant E-selectin at 4 °C overnight. The error bars show the standard deviations determined by at least four separate experiments.

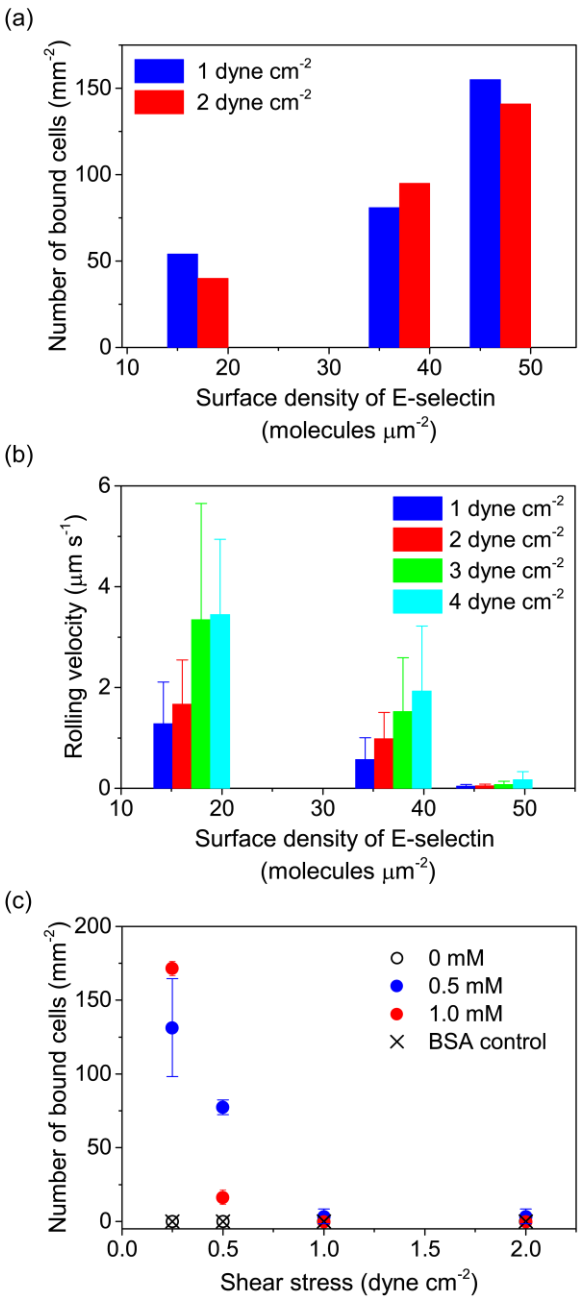

Supplementary Figure 2. Characterization of the rolling behaviour of KG1a cells on E-selectin. (a) Number of bound cells to the E-selectin surface at different surface densities of the deposited rh E-selectin. The cells were injected into the microfluidic chambers at the shear stresses of either 1 or 2 dyne cm^{-2}. (b) Rolling velocity of the cells on the E-selectin surface at different

surface densities of the deposited rh E-selectin. The cells were injected into the microfluidic chambers at the shear stresses of either 1, 2, 3 or 4 dyne cm^{-2}. The error bars show the standard deviations determined by at least six separate experiments. (c) Number of bound cells to the E-selectin surface at different applied shear stresses. The cells were injected into the microfluidic chambers at the calcium ion concentrations of either 0, 0.5 or 1.0 mM. BSA control (i.e. no E-selectin on the surface) is included as a negative control. The error bars show the standard deviations determined by at least three separate experiments.

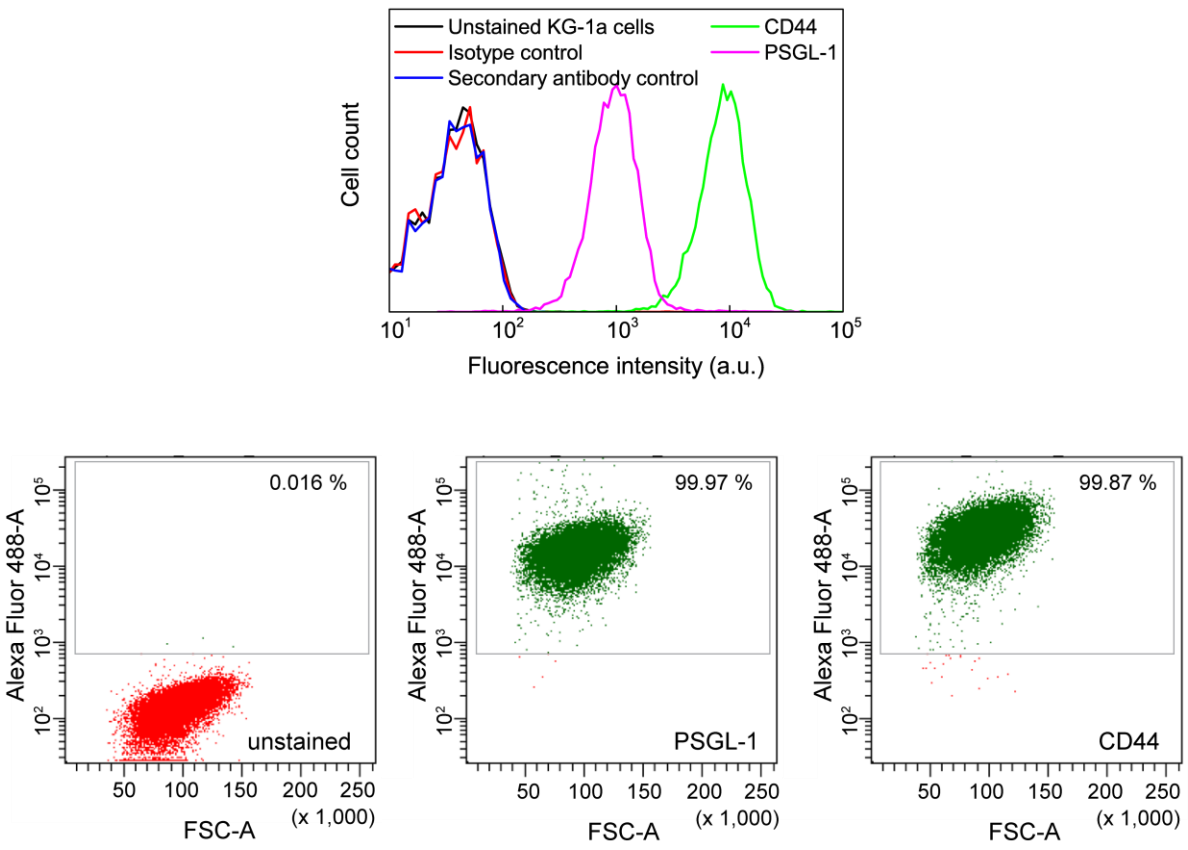

Supplementary Figure 3. Flow cytometric analysis of the binding specificity of CD44 and PSGL-1 antibodies. CD44 (green) and PSGL-1 (magenta) on KG1a cells were immunostained by antibodies against CD44 and PSGL-1 (clone 515 for CD44 and clone KPL-1 for PSGL-1) and Alexa-Fluor-488-conjugated secondary antibody against the isotype of the CD44 and PSGL-1 antibodies (goat anti-mouse IgG). Unstained KG1a cells (black), isotype control labelled cells (red), and secondary alone-labelled cells (blue) were included as controls. This is a representative experiment of n=2 independent experiments.

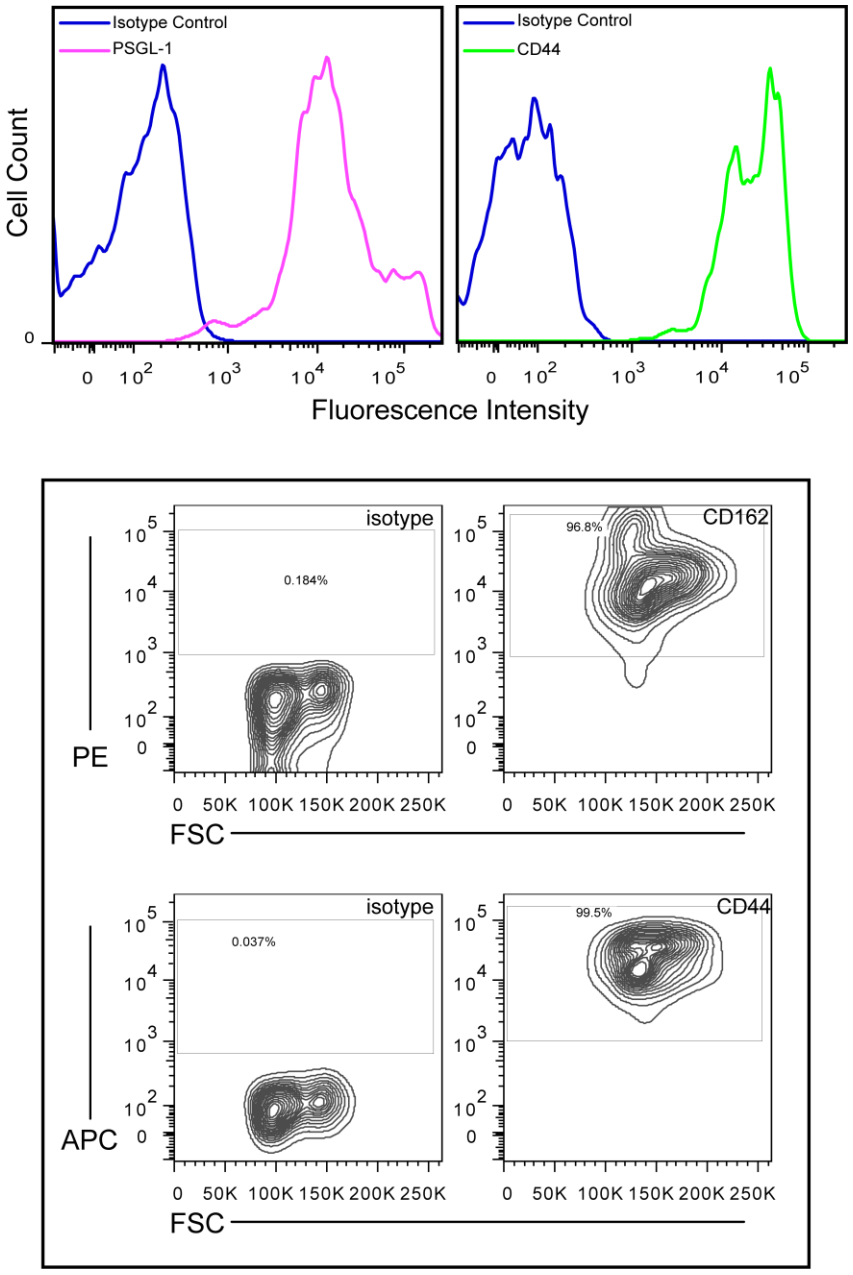

Supplementary Figure 4. Assessment of E-selectin ligand expression on human CD34^{pos}-HSPCs. Primary human CD34^{pos}-HSPCs were stained for CD44 (green) and PSGL-1 (magenta) using antibodies specific to these antigens (anti-human CD44, clone 2C5 and anti-human PSGL-1, clone KPL-1) and analyzed by flow cytometry (FACS Canto and FlowJo). This is a representative experiment of n=2 independent experiments.

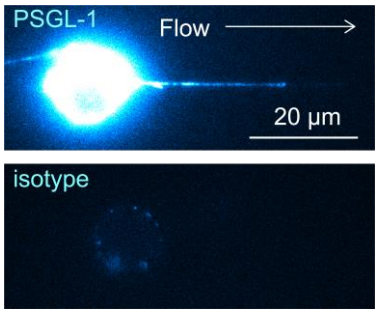

Supplementary Figure 5. Binding specificity of the antibody characterized by fluorescence imaging. (top) Fluorescence image of PSGL-1 molecules on a KG1a cell that were immunostained by Alexa-Fluor-555-conjugated antibody (anti-PSGL-1 antibody, clone KPL-1). The labelled cells were injected into microfluidic chambers whose surface was coated by the rh E-selectin molecules at a density of 15 molecules μm^{-2}. The cells were injected into the chambers at a shear stress of 2 dyne cm^{-2}. (bottom) Fluorescence image of an isotype control labelled KG1a cell that was injected into the fluidic chambers at conditions identical to those for the PSGL-1 immunostained cells.

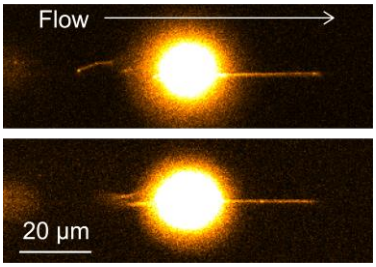

Supplementary Figure 6. Formation of tethers and slings on KG1a cells while rolling over E-selectin. Examples of the fluorescence images of the cell membrane (stained by Vybrant DiO dye) captured during cell rolling over the surface-deposited E-selectin molecules. The stained cells were injected into the microfluidic chambers whose surface was coated with rh E-selectin molecules at a density of 15 molecules μm^{-2}. The cells were injected into the chambers at a shear stress of 2 dyne cm^{-2}.

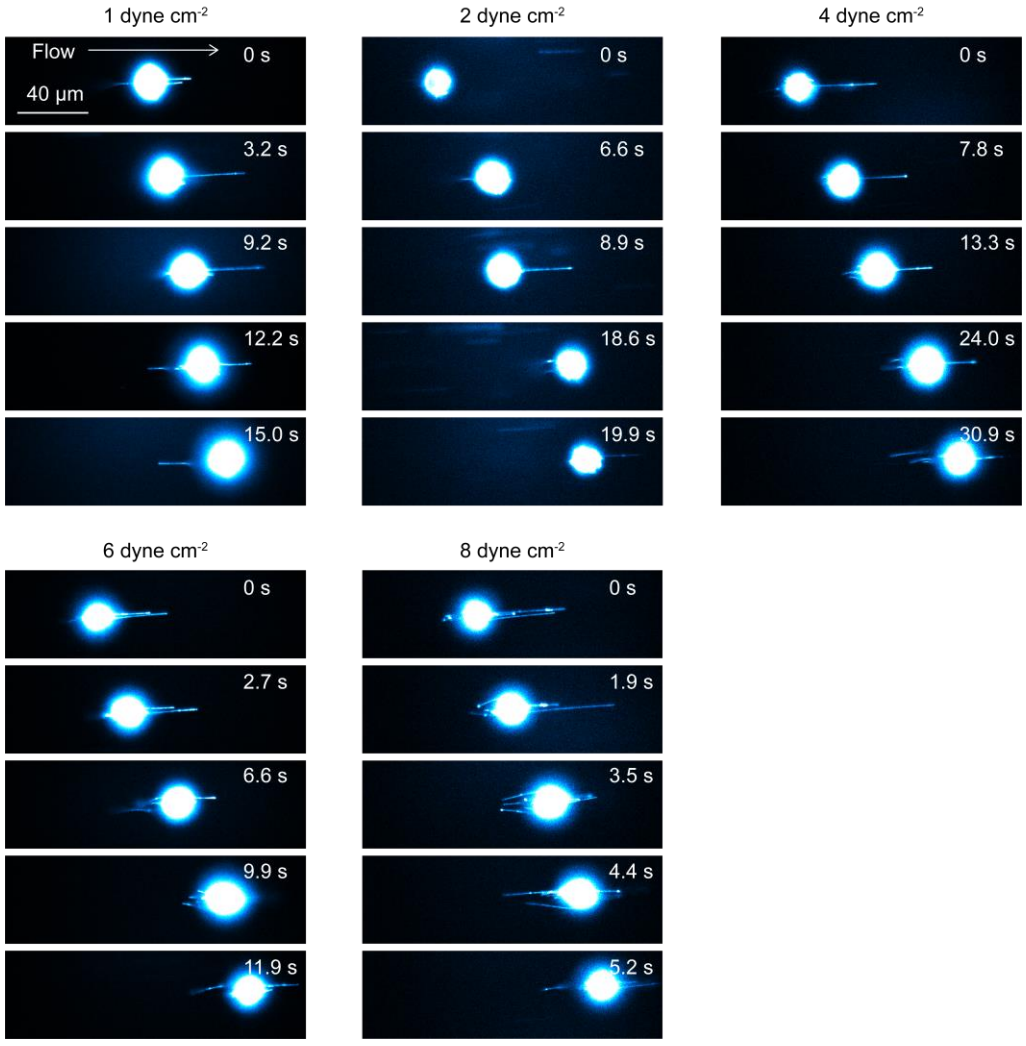

Supplementary Figure 7. Shear force-dependent formation of the tethers and slings on KG1a cells rolling over E-selectin. Time-lapse fluorescence images of CD44 (immunostained by Alexa-Fluor-647-conjugated anti-CD44 antibody clone 515) captured during cell rolling over the surface-deposited E-selectin molecules. The labelled cells were injected into the microfluidic chambers whose surface was coated with rh E-selectin molecules at a density of 15 molecules μm^{-2}. The cells were injected into the chambers at a shear stress of 1, 2, 4 or 8 dyne cm^{-2}.

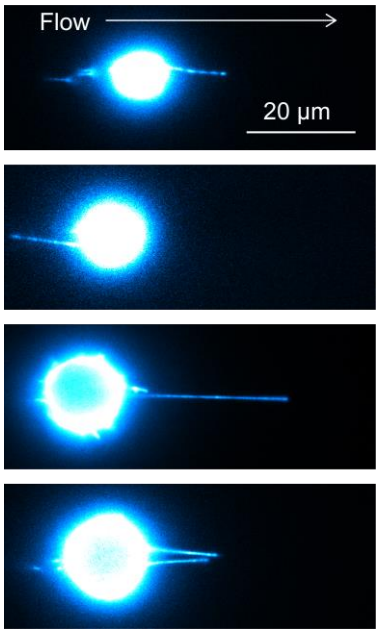

Supplementary Figure 8. Formation of the tethers and slings on primary human CD34^{pos}-HSPCs rolling over E-selectin. Examples of the fluorescence images of CD44 (immunostained by Alexa-Fluor-647-conjugated anti-CD44 antibody, clone 515) captured during human CD34pos-HSPC rolling over the surface-deposited E-selectin molecules. The labelled cells were injected into the microfluidic chambers whose surface was coated with rh E-selectin molecules at a density of 15 molecules µm^{-2}. The cells were injected into the chambers at a shear stress of 2 dyne cm^{-2}.

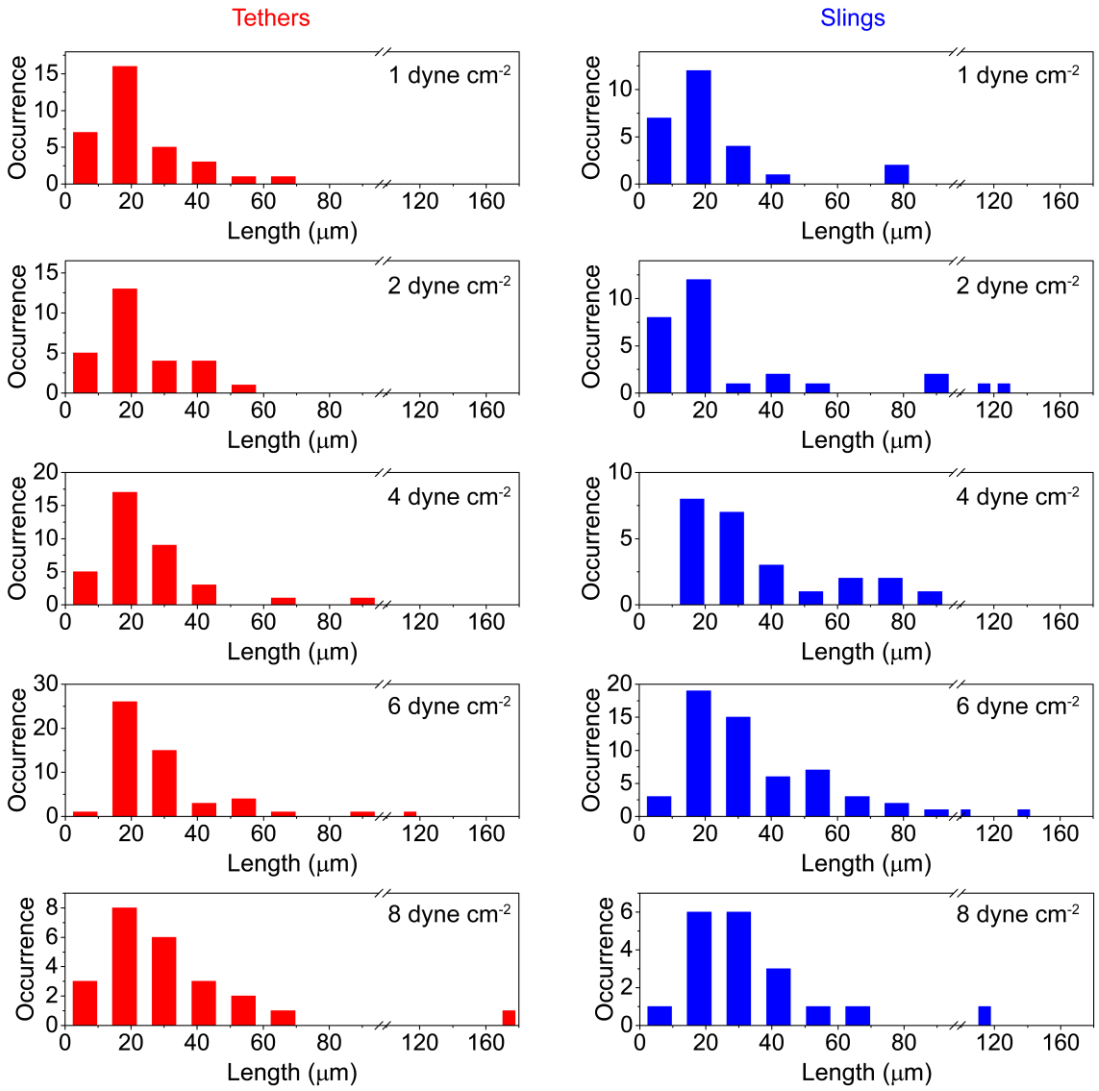

Supplementary Figure 9. Length of the tethers and slings formed on KG1a cells rolling over E-selectin. Frequency histograms of the length of tethers (red bars) and slings (blue bars) formed during the KG1a cells rolling over E-selectin. The cells were injected into the microfluidic chambers whose surface was coated with rh E-selectin molecules at a density of 15 molecules μm^{-2}. The cells were injected into the chambers at shear stress of 1, 2, 4 or 8 dyne cm^{-2} as indicated.

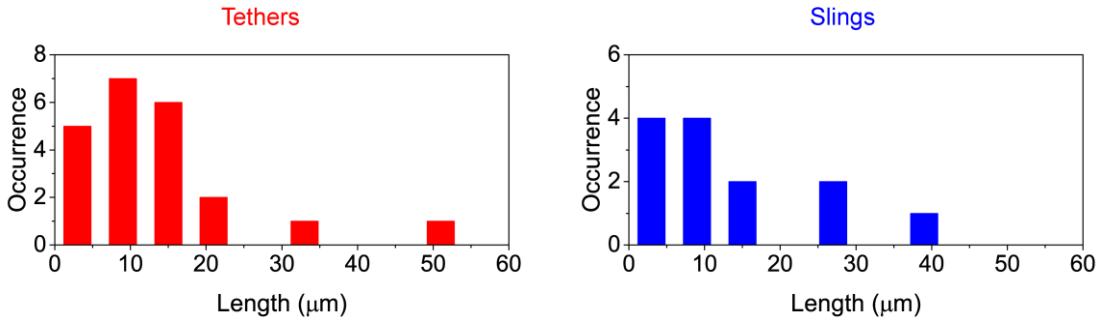

Supplementary Figure 10. Length of the tethers and slings formed on primary human CD34^{pos}-HSPCs rolling over E-selectin. Frequency histograms of the length of tethers (red bars) and slings (blue bars) formed during the primary human CD34^{pos}-HSPCs rolling over E-selectin. The cells were injected into the microfluidic chambers whose surface was coated with rh E-selectin molecules at a density of 15 molecules μm^{-2}. The cells were injected into the chambers at a shear stress of 2 dyne cm^{-2} as indicated.

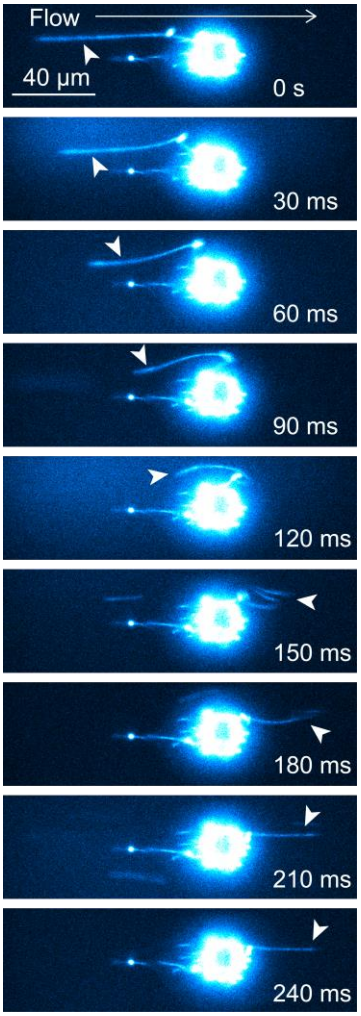

Supplementary Figure 11. Conversion of tethers into slings observed for KG1a cells rolling over E-selectin. Time-lapse fluorescence images of CD44 (immunostained by Alexa-Fluor-647-conjugated anti-CD44 antibody, clone 515) captured during cell rolling over the surface-deposited E-selectin molecules. The arrow heads show a tether that is converted into a sling upon the detachment of the tethering point from the E-selectin surface. The cells were injected into the microfluidic chambers whose surface was coated with rh E-selectin molecules at a density of 15 molecules μm^{-2}. The cells were injected into the chambers at a shear stress of 6 dyne cm^{-2}.

Supplementary Figure 12. Conversion of a tether into sling observed for a primary human CD34^{pos}-HSPC rolling over E-selectin. Time-lapse fluorescence images of CD44 (immunostained by Alexa-Fluor-647-conjugated anti-CD44 antibody, clone 515) captured during cell rolling over the surface-deposited E-selectin molecules. The arrow heads show the tether that is converted into sling upon the detachment of the tethering point from the E-selectin surface. The cells were injected into the microfluidic chambers whose surface was coated with rh E-selectin molecules at a density of 15 molecules µm^{-2}. The cells were injected into the chambers at a shear stress of 2 dyne cm^{-2}.

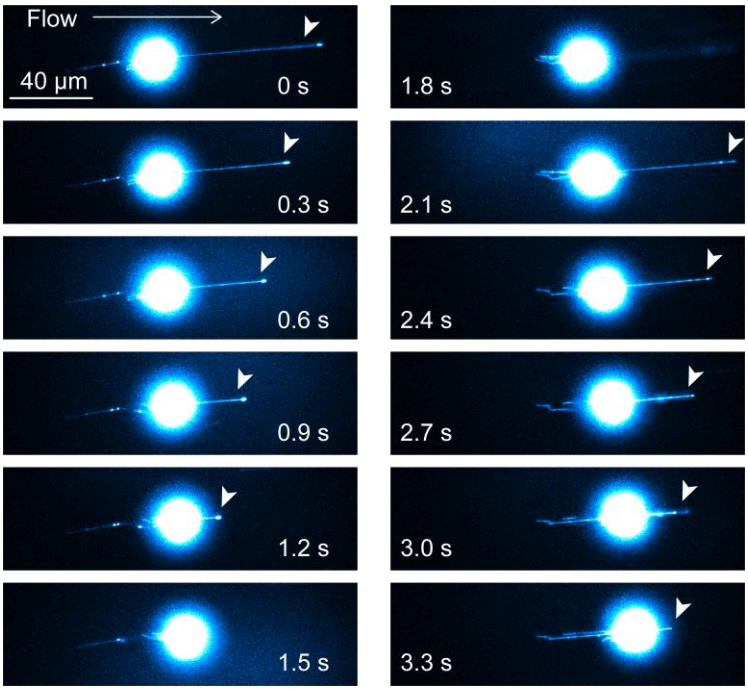

Supplementary Figure 13. Retraction of the slings. Time-lapse fluorescence images of CD44 (immunostained by Alexa-Fluor-647-conjugated anti-CD44 antibody, clone 515) captured during cell rolling over the surface-deposited E-selectin molecules. The arrow heads show the slings with this retraction behaviour. The cells were injected into the microfluidic chambers whose surface was coated with rh E-selectin molecules at a density of 15 molecules μm^{-2}. The cells were injected into the chambers at a shear stress of 8 dyne cm^{-2}.

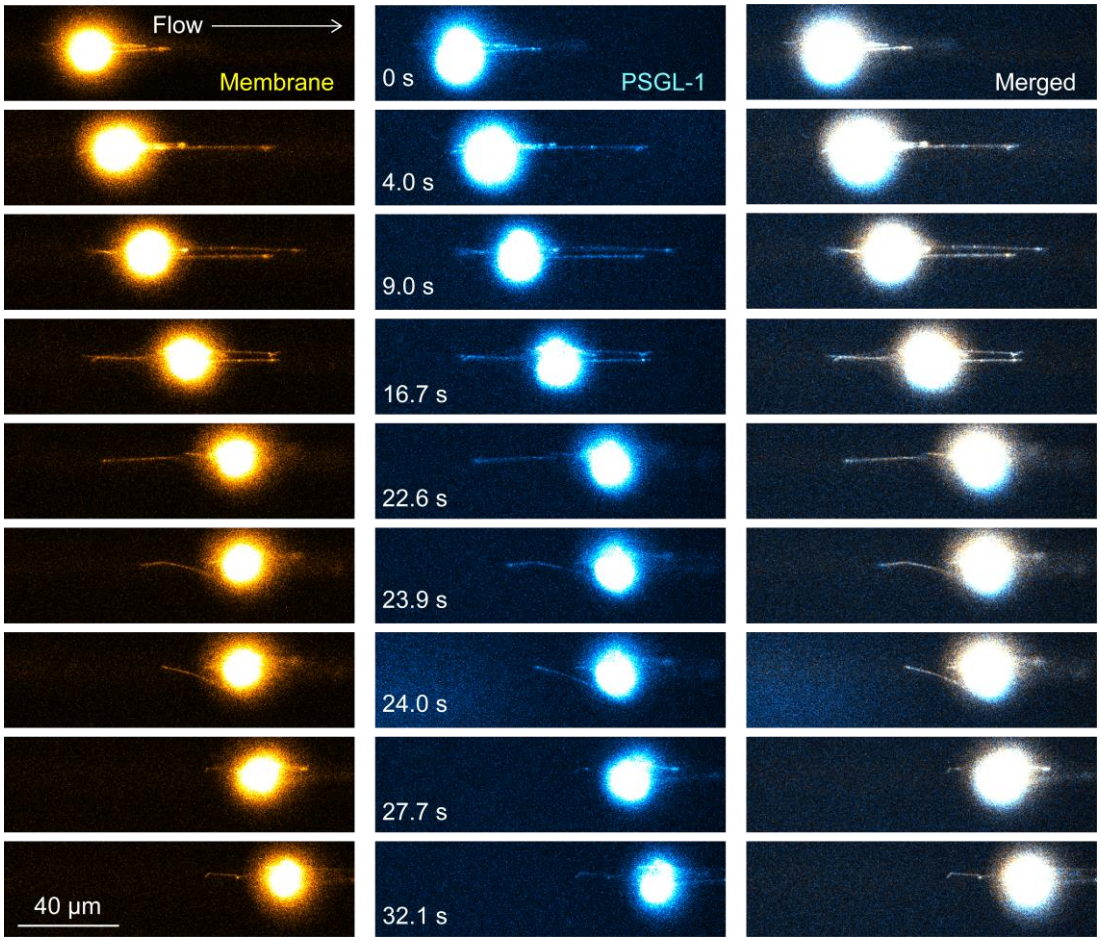

Supplementary Figure 14. Colocalisation of cell membrane and PSGL-1 on the tethers and slings formed on a KG1a cell rolling over E-selectin. Time-lapse fluorescence images of the cell membrane (yellow, stained by Vybrant DiO dye) and PSGL-1 (cyan, immunostained by Alexa-Fluor-647-conjugated anti-PSGL-1 antibody, clone KPL-1) captured during cell rolling over the surface-deposited E-selectin molecules. The merged images are displayed in the right panels. The stained and labelled cells were injected into the microfluidic chambers whose surface was coated with rh E-selectin molecules at a density of 15 molecules μm^{-2}. The cells were injected into the chambers at a shear stress of 2 dyne cm^{-2}.

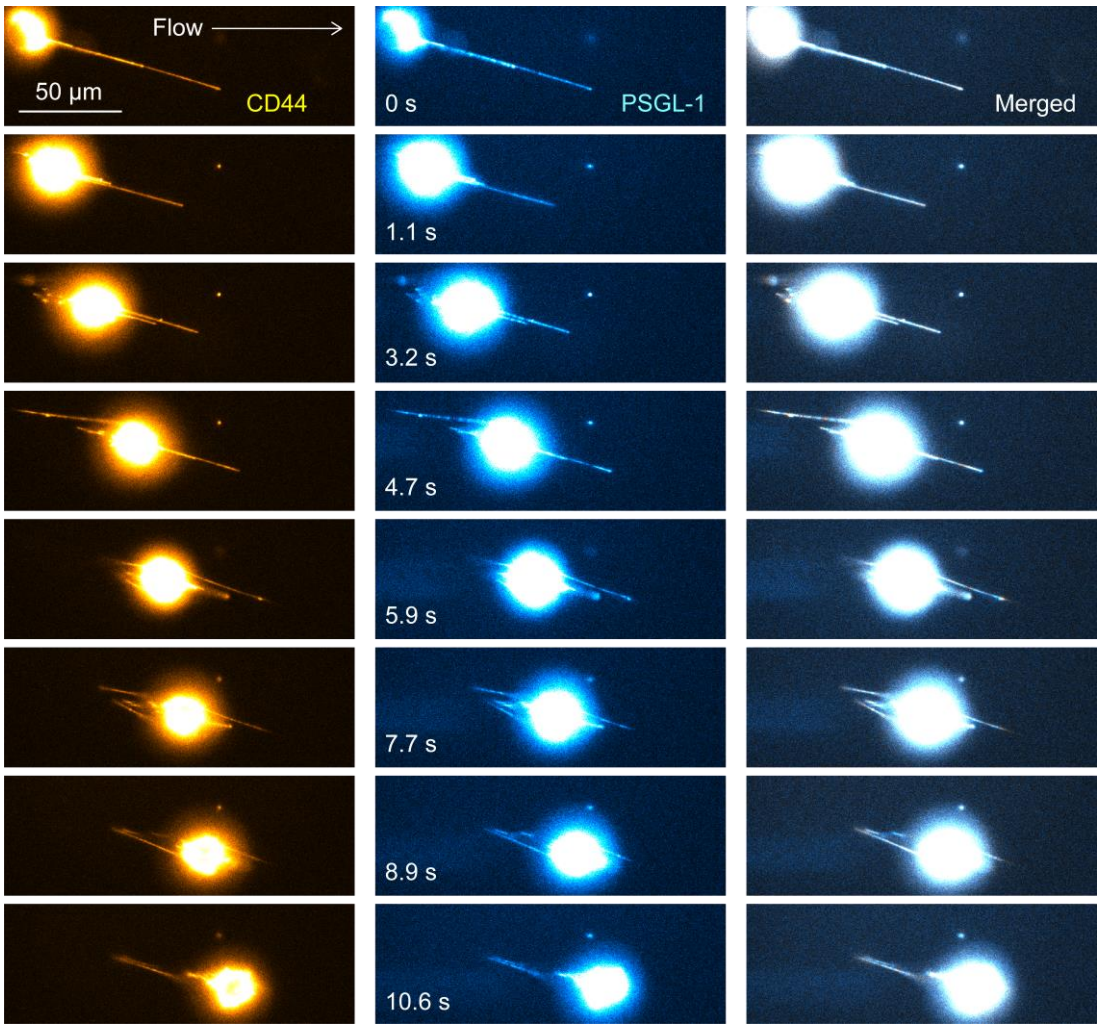

Supplementary Figure 15. Colocalisation of CD44 and PSGL-1 on the tethers and slings formed on a KG1a cell rolling over E-selectin. Time-lapse fluorescence images of CD44 (yellow, immunostained by Alexa-Fluor-647-conjugated anti-CD44 antibody, clone 515) and PSGL-1 (cyan, immunostained by Alexa-Fluor-488-conjugated anti-PSGL-1 antibody, clone KPL-1) captured during cell rolling over the surface-deposited E-selectin molecules. The merged images are displayed in the right panels. The labelled cells were injected into the microfluidic chambers whose surface was coated with rh E-selectin molecules at a density of 15 molecules µm^{-2}. The cells were injected into the chambers at a shear stress of 2 dyne cm^{-2}.

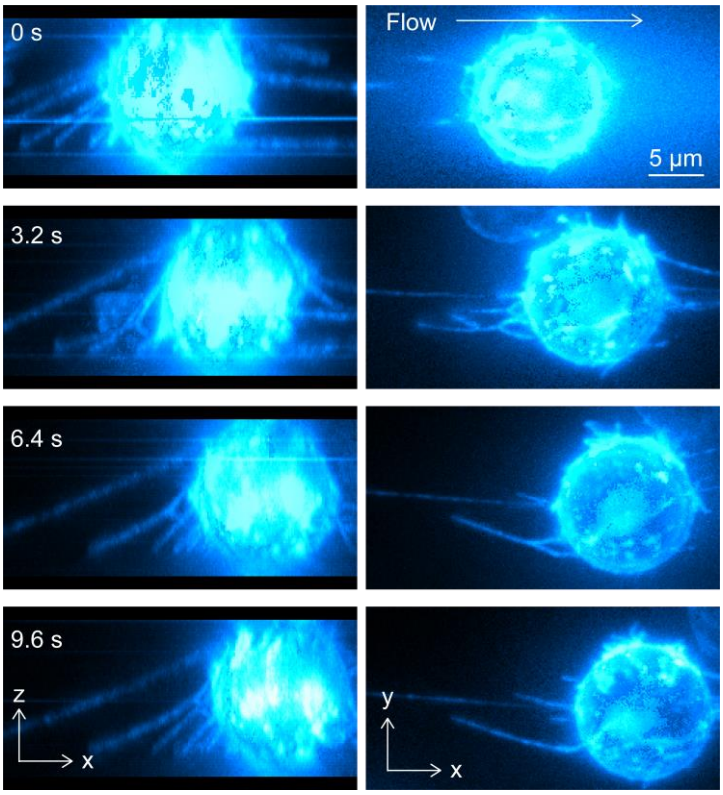

Supplementary Figure 16. 3D views of the tethers and slings formed on a KG1a cell rolling over E-selectin by CD44. Side view (left) and top view (right) of the 3D reconstructed time-lapse fluorescence images of CD44 (immunostained by Alexa-Fluor-647-conjugated anti-CD44 antibody, clone 515) captured during cell rolling over the surface-deposited E-selectin molecules. The 3D images were reconstructed by recording fluorescence images of the cell at 53 different Z-axis positions with 0.5 µm step size. The single 3D images were therefore captured every 1.6 sec (30 ms exposure time at each Z-position). The labelled cells were injected into the microfluidic chambers whose surface was coated with rh E-selectin molecules at a density of 15 molecules μm^{-2}. The cells were injected into the chambers at a shear stress of 2 dyne cm^{-2}.

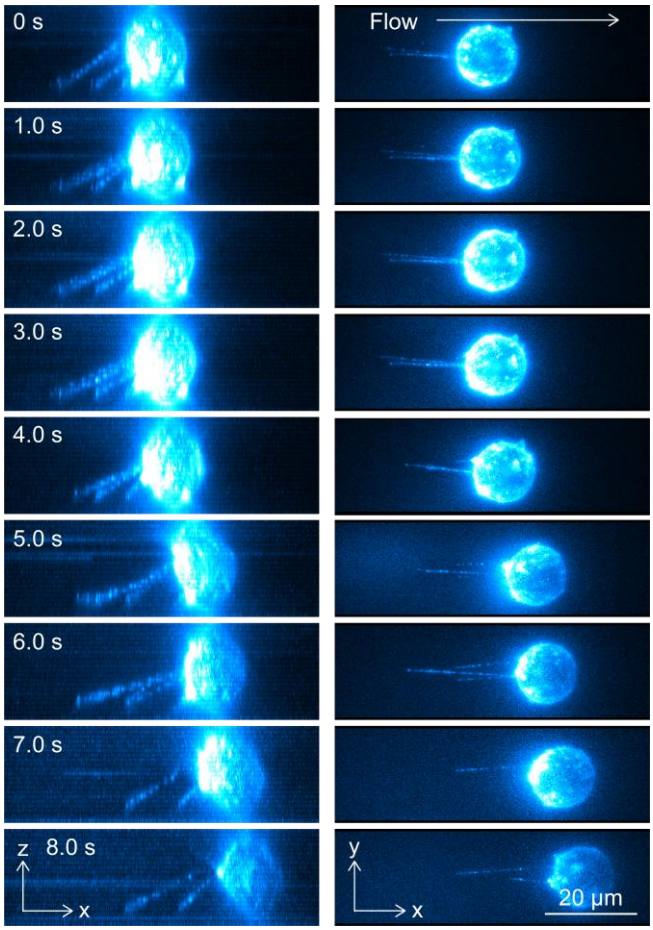

Supplementary Figure 17. 3D views of the tethers formed on a KG1a cell rolling over E-selectin by PSGL-1. Side view (left) and top view (right) of the 3D reconstructed time-lapse fluorescence images of PSGL-1 (immunostained by Alexa-Fluor-555-conjugated anti-PSGL-1 antibody, clone KPL-1) captured during cell rolling over surface-deposited E-selectin molecules. The 3D images were reconstructed by recording fluorescence images of the cell at 33 different Z-axis positions with 1.0 µm step size. The single 3D images were therefore captured every 1.0 sec (30 ms exposure time at each Z-position). The labelled cells were injected into the microfluidic chambers whose surface was coated with rh E-selectin molecules at a density of 15 molecules μm^{-2}. The cells were injected into the chambers at a shear stress of 2 dyne cm^{-2}.

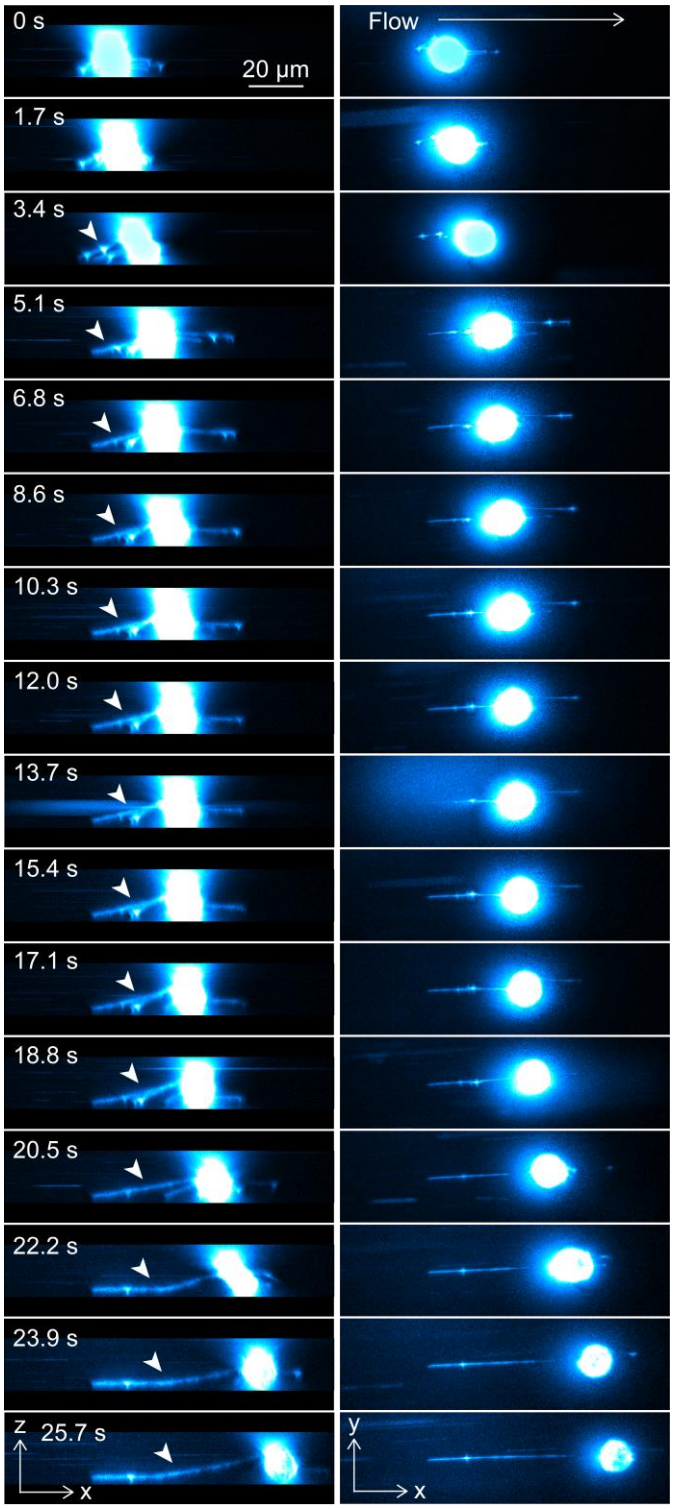

Supplementary Figure 18. 3D views of the elongation of the tether formed on a KG1a cell rolling over E-selectin. Side view (left) and top view (right) of the 3D reconstructed time-lapse

fluorescence images of CD44 (immunostained by Alexa-Fluor-488-conjugated anti-CD44 antibody, clone 515) captured during cell rolling over surface-deposited E-selectin molecules. The 3D images were reconstructed by recording fluorescence images of the cell at 57 different Z-axis positions with 0.5 μm step size. The single 3D images were therefore captured every 1.7 sec (30 ms exposure time at each Z-position). The arrowheads indicate the tether that shows elongation behaviour. The labelled cells were injected into the microfluidic chambers whose surface was coated with rh E-selectin molecules at a density of 15 molecules μm^{-2}. The cells were injected into the chambers at a shear stress of 2 dyne cm^{-2}.

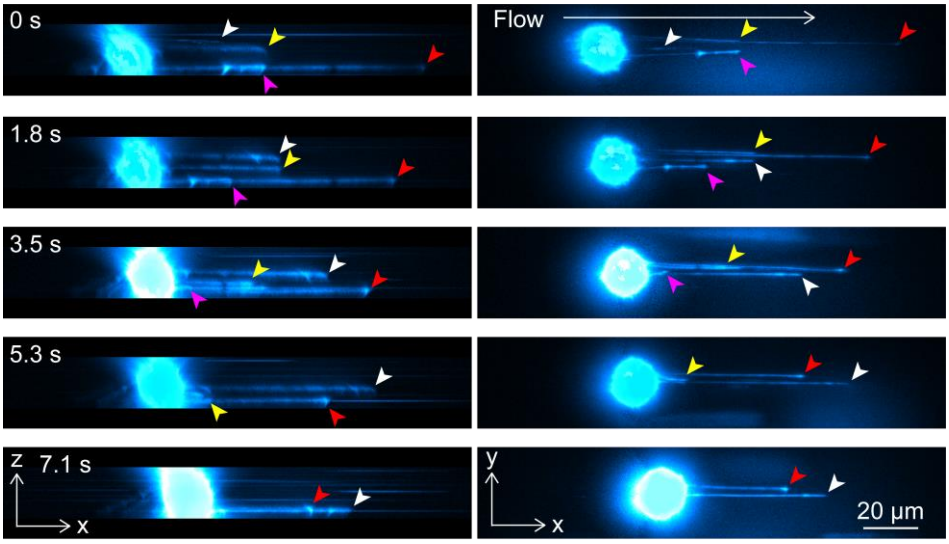

Supplementary Figure 19. 3D views of the slings formed on a KG1a cell that show changes in the Z-axis positions during cell rolling over E-selectin. Side view (left) and top view (right) of the 3D reconstructed time-lapse fluorescence images of CD44 (immunostained by Alexa-Fluor-488-conjugated anti-CD44 antibody, clone 515) captured during cell rolling over the surface-deposited E-selectin molecules. The 3D images were reconstructed by recording fluorescence images of the cell at 59 different Z-axis positions with 0.5 µm step size. The single 3D images were therefore captured every 1.8 sec (30 ms exposure time at each Z-position). The arrow heads in white, yellow, red and magenta show four different slings formed during cell rolling. The labelled cells were injected into microfluidic chambers whose surface was coated with rh E-selectin molecules at a density of 15 molecules μm^{-2}. The cells were injected into the chambers at a shear stress of 2 dyne cm^{-2}.

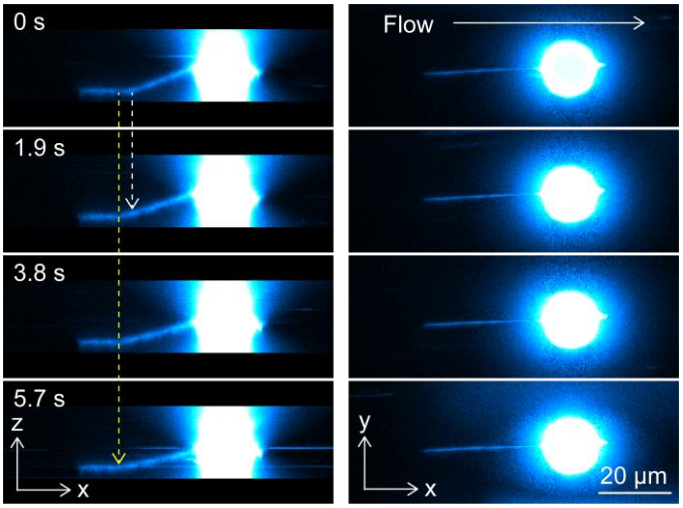

Supplementary Figure 20. 3D views of the tether formed on a KG1a cell that show changes in the position of the anchoring points during cell rolling over E-selectin. Side view (left) and top view (right) of the 3D reconstructed time-lapse fluorescence images of CD44 (immunostained by Alexa-Fluor-488-conjugated anti-CD44 antibody, clone 515) captured during cell rolling over the surface-deposited E-selectin molecules. The 3D images were reconstructed by recording fluorescence images of the cell at 63 different Z-axis positions with 0.5 µm step size. The single 3D images were therefore captured every 1.9 sec (30 ms exposure time at each Z-position). The white and yellow arrows show the positions of the two anchoring points formed on the tether. The first anchoring point (white arrow) is detached during cell rolling, whereas the second anchoring point (yellow arrow) continues attaching to the surface E-selectin. The labelled cells were injected into the microfluidic chambers whose surface was coated with rh E-selectin molecules at a density of 15 molecules μm^{-2}. The cells were injected into the chambers at a shear stress of 2 dyne cm^{-2}.

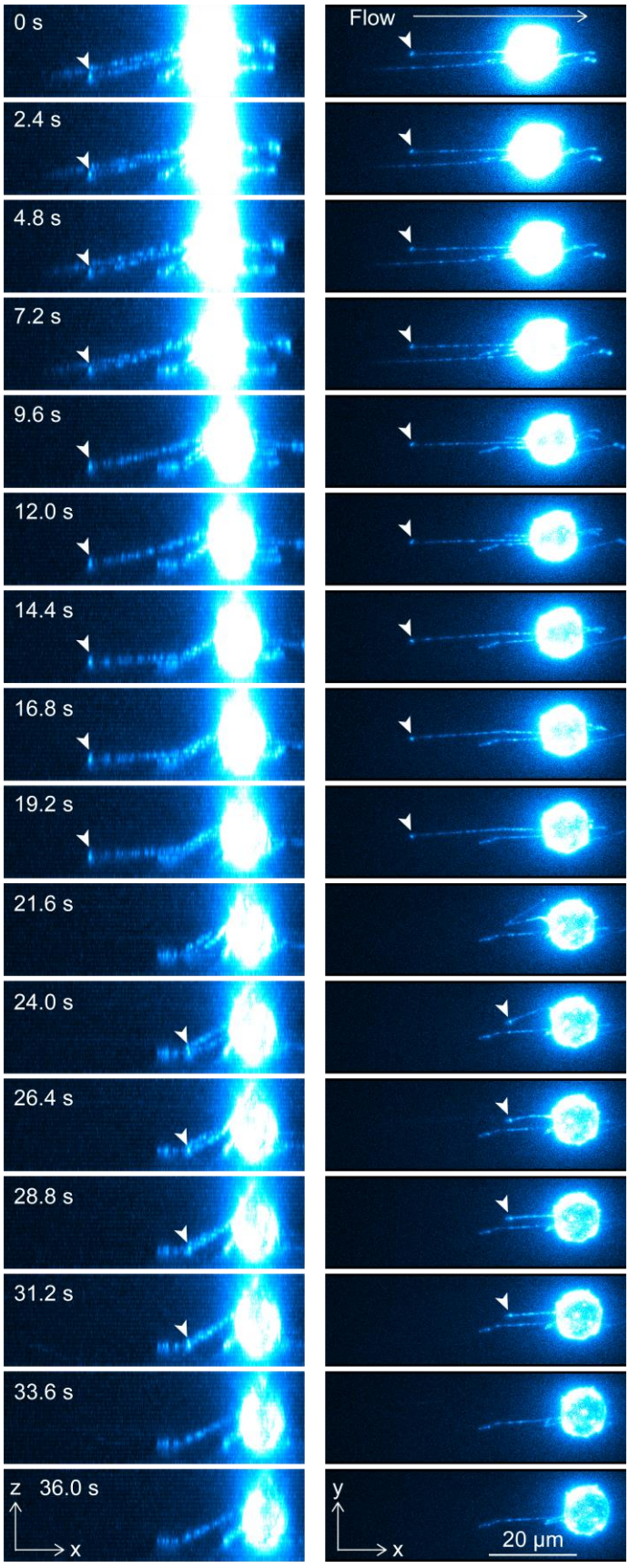
0 s
2.4 s
4.8 s
7.2 s
9.6 s
12.0 s
14.4 s
16.8 s
19.2 s
21.6 s
24.0 s
26.4 s
28.8 s
31.2 s
33.6 s
z 36.0 s
x
Flow
y
x
20 µm

Supplementary Figure 21. 3D views of the tethers and slings formed on a KG1a cell that demonstrates clustering behaviour of PSGL-1 at the tethering points during cell rolling over E-selectin. Side view (left) and top view (right) of the 3D reconstructed time-lapse fluorescence images of PSGL-1 (immunostained by Alexa-Fluor-555-conjugated anti-PSGL-1 antibody, clone KPL-1) captured during cell rolling over the surface-deposited E-selectin molecules. The 3D images were reconstructed by recording fluorescence images of the cell at 40 different Z-axis positions with 1.0 μm step size. The single 3D images were therefore captured every 1.2 sec (30 ms exposure time at each Z-position). The arrowheads show the bright fluorescence spots of PSGL-1 (i.e. clusters of PSGL-1) found at the tethering points. The labelled cells were injected into the microfluidic chambers whose surface was coated with rh E-selectin molecules at a density of 15 molecules μm^{-2}. The cells were injected into the chambers at a shear stress of 2 dyne cm^{-2}.

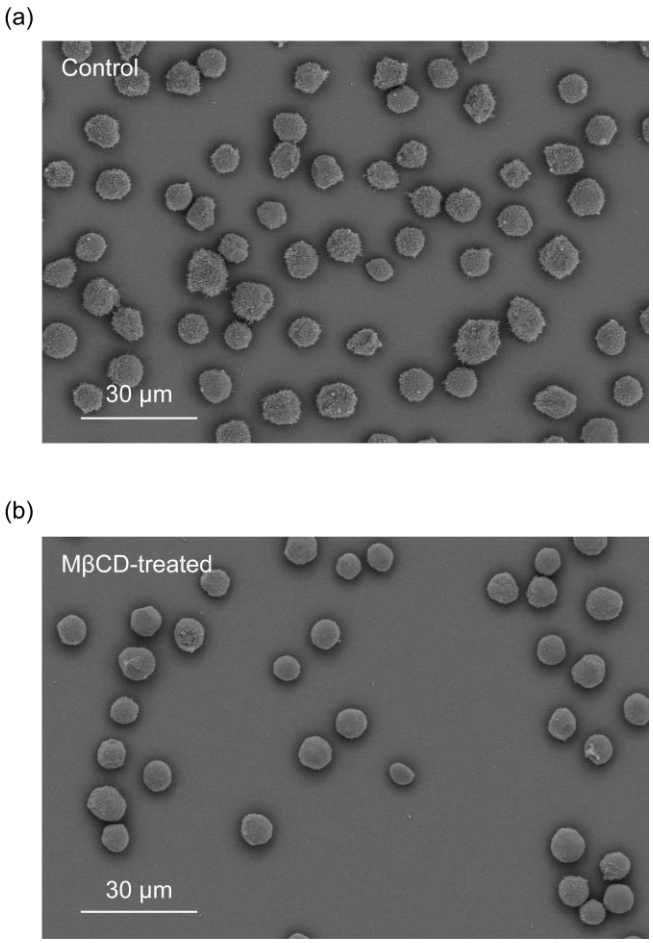

Supplementary Figure 22. Scanning electron microscopy (SEM) images of KG1a cells. SEM images of (a) control and (b) methyl-β-cyclodextrin (MβCD)-treated KG1a cells. These are representative images of n=2 independent experiments.

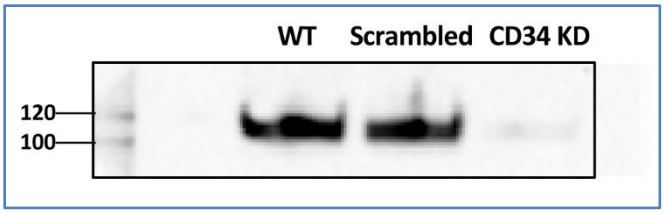

Supplementary Figure 23. CD34 knockdown in KG1a cells. KG1a cells were transfected with either a scrambled control siRNA (Silencer Select, Life technologies; 4390843) or with siRNA specific for CD34 (Select, Life technologies; 4392420-s2644). Cells were collected after 48 h of transfection and subjected to Western blot analysis for CD34 protein expression. Lane 1: untreated KG1a cells; Lane 2: scrambled negative control siRNA; Lane 3: CD34 KD KG1a cells. Membrane bands were normalized using total cells protein. This is representative of n=5 independent experiments.

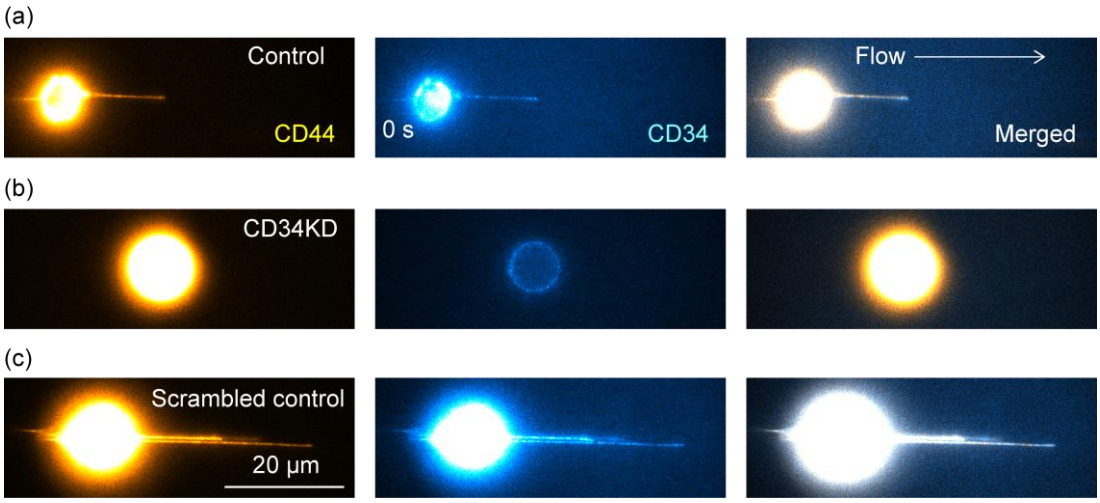

Supplementary Figure 24. Effect of the knockdown of CD34 on the formation of tethers and slings on KG1a cells while rolling over E-selectin. Examples of the two-colour fluorescence images of CD34 (cyan, immunostained by Alexa-Fluor-488-conjugated anti-CD34 antibody clone QBEND/10) and CD44 (yellow, immunostained by Alexa-Fluor-647-conjugated anti-CD44 antibody clone 515) on (a) control KG1a cell, (b) KG1a cell transfected with siRNA specific for CD34, and (c) KG1a cell transfected with scrambled control siRNA captured during cell rolling over the surface-deposited E-selectin molecules. The stained cells were injected into the microfluidic chambers whose surface was coated with rh E-selectin molecules at a density of 15 molecules μm^{-2}. The cells were injected into the chambers at a shear stress of 2 dyne cm^{-2}. These images were captured using identical imaging conditions and were shown in an identical image contrast.

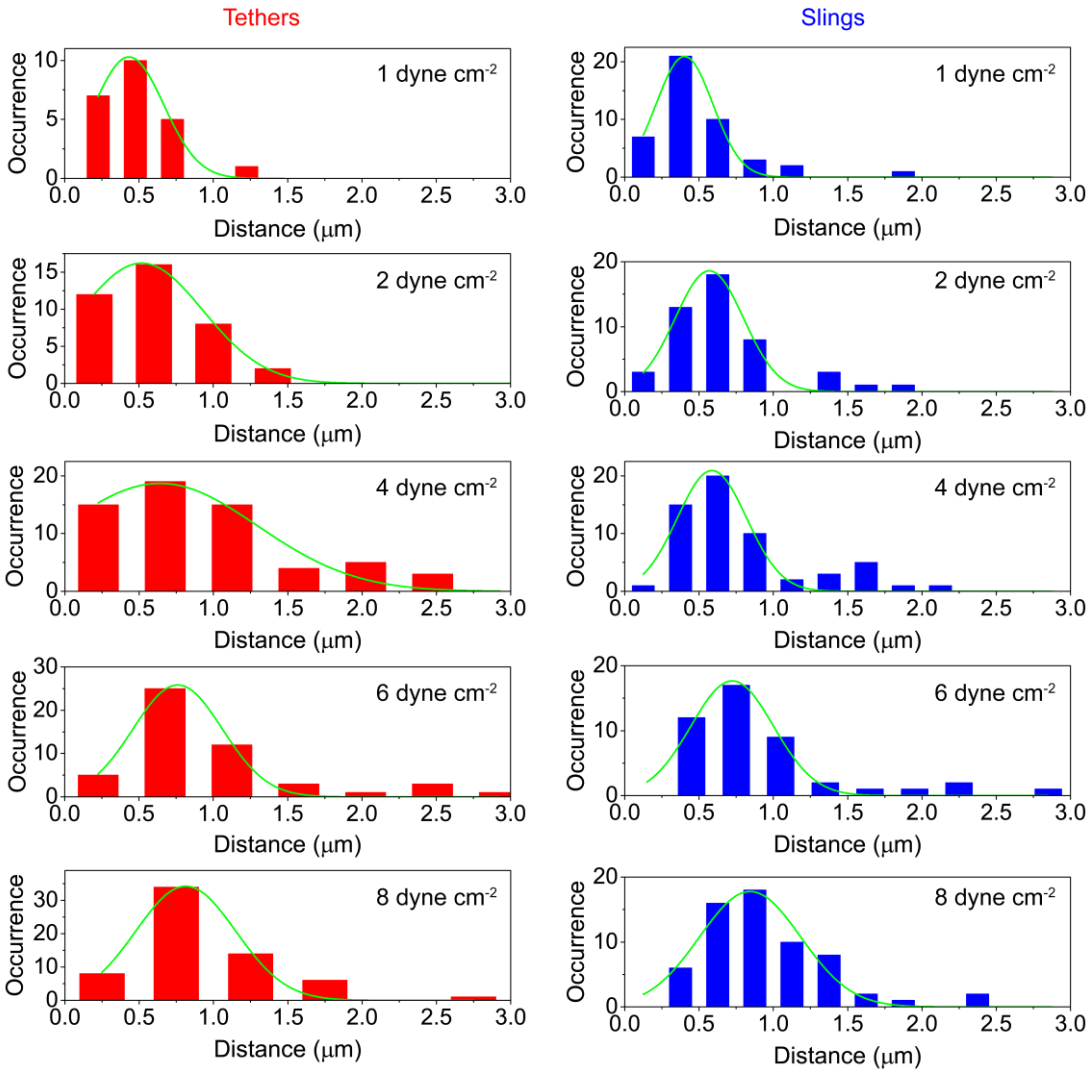

Supplementary Figure 25. Distance between the PSGL-1 spots on the tethers and slings formed on KG1a cells rolling over E-selectin. Frequency histograms of the distance between the adjacent fluorescent spots of PSGL-1 (immunostained by Alexa-Fluor-555-conjugated anti-PSGL-1 antibody, clone KPL-1) on the tethers (red bars) and slings (blue bars) formed during the KG1a cells rolling over E-selectin. The cells were injected into microfluidic chambers whose surface was coated with rh E-selectin molecules at a density of 15 molecules μm^{-2}. The cells were injected into the chambers at a shear stress of either 1, 2, 4 or 8 dyne cm^{-2}.

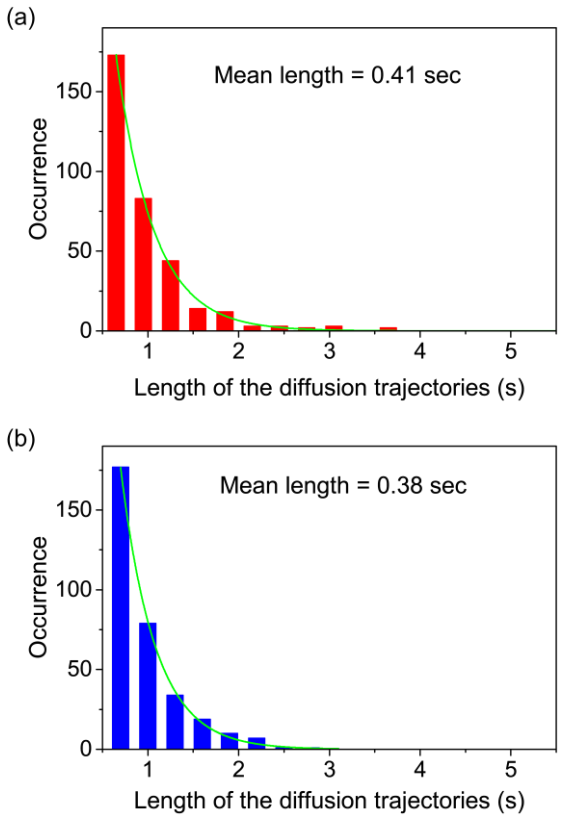

Supplementary Figure 26. Length of the single-molecule diffusion trajectories of the PSGL-1 molecules on the tethers and slings formed on KG1a cells rolling over E-selectin. Frequency histograms of the length of the single-molecule diffusion trajectories of PSGL-1 molecules (immunostained by Alexa-Fluor-555-conjugated anti-PSGL-1 antibody, clone KPL-1) that show diffusional motion on the (a) tethers and (b) slings formed during the KG1a cells rolling over E-selectin. The solid lines show the fitting to single-exponential decaying function. The mean trajectory lengths (0.41s and 0.38 s for the trajectories obtained from the tethers and slings, respectively) were calculated using the decay constants obtained by the fits. The cells were injected into microfluidic chambers whose surface was coated with rh E-selectin molecules at a density of 15 molecules μm^{-2}. The cells were injected into the chambers at a shear stress of 2 dyne cm^{-2}.

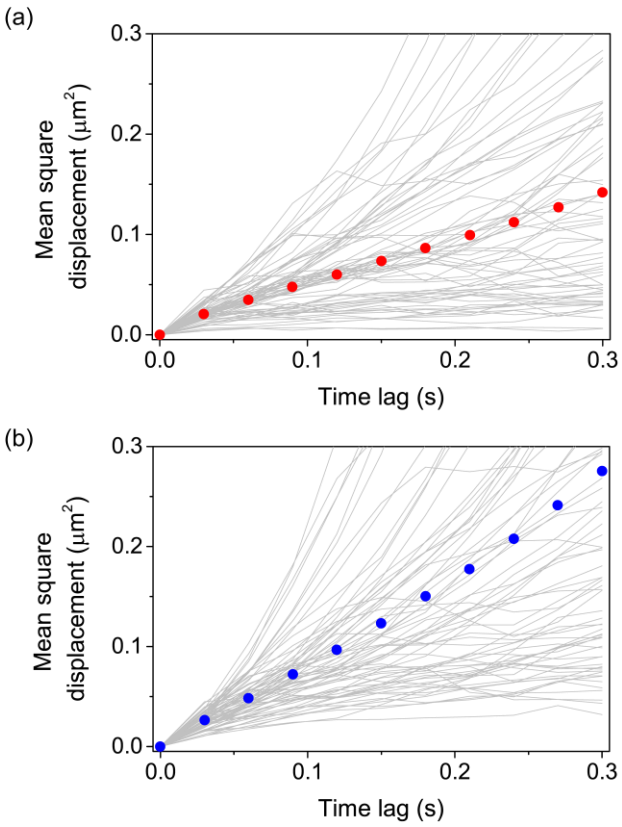

Supplementary Figure 27. MSD vs time-lag plots obtained from the single-molecule diffusion trajectories of PSGL-1 on the tethers and slings. MSD vs time-lag plots obtained for PSGL-1 molecules (immunostained by Alexa-Fluor-555-conjugated anti-PSGL-1 antibody, clone KPL-1) that show diffusional motion on the (a) tethers and (b) slings formed during KG1a cells rolling over E-selectin. The grey lines show individual MSD vs time-lag plots obtained from individual single-molecule diffusion trajectories. The red and blue dots show mean MSD vs time-lag plots for the tethers and slings, respectively. The cells were injected into microfluidic chambers whose surface was coated with recombinant E-selectin molecules at a density of 15 molecules μm^{-2}. The cells were injected into the chambers at a shear stress of 2 dyne cm^{-2}.

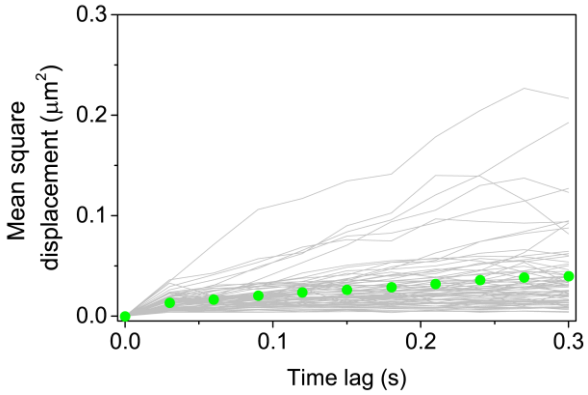

Supplementary Figure 28. MSD vs time-lag plots obtained from the single-molecule diffusion trajectories of PSGL-1 localised on microvilli. MSD vs time-lag plots obtained for PSGL-1 molecules (immunostained by Alexa-Fluor-488-conjugated anti-PSGL-1 antibody, clone KPL-1) that are localised on microvilli in the control KG1a cells. The grey lines show individual MSD vs time-lag plots obtained from individual single-molecule diffusion trajectories. The green dots show mean MSD vs time-lag plot. The cells were injected into uncoated microfluidic chambers without any recombinant E-selectin molecules. The fluorescence images were captured in the absence of any external shear stress.

Supplementary Table

Supplementary Table 1. Calculated volumetric flow rates (*Q*) required for obtaining the experimental shear stresses (τ) using the µ-slide VI $^{0.1}$ microfluidic chamber.

τ (dyne cm^{-2})	Q (µl min^{-1})
1.0	10.0
2.0	20.0
4.0	40.0
6.0	60.0
8.0	80.0

The volumetric flow rates were calculated using the formula, $\tau = 6\mu Q/a^2 b$, where µ denotes viscosity of the medium (1×10^{-3} Pa s for water). a and b are the height and width of the channel ($a = 1 \times 10^{-4}$ m and $b = 1 \times 10^{-3}$ m for the µ-slide VI $^{0.1}$ microfluidic chamber).

Supplementary Notes

1. Bivalency effect of the antibodies

Antibodies have two binding sites to their epitopes. This may cause artificial clustering of the labelled molecules. Since we observed the discrete spatial distribution of the PSGL-1 molecule on the tethers and slings of the KG1a cell that are formed during the cell rolling over E-selectin, we investigated if this spatial distribution is a result of the artificial clustering of the immunostained PSGL-1 molecules due to the bivalency effect of the anti-PSGL-1 antibody. To that end, we immunostained PSGL-1 on KG1a cells using the Alexa-Fluor-555-conjugated Fab fragment of the anti-PSGL-1 antibody that has only one binding site to its epitope. The immunofluorescence image of PSGL-1 on the tethers and slings of the KG1a cells obtained using the Alexa-Fluor-555-conjugated Fab fragment of the anti-PSGL-1 antibody showed a spatial distribution of the PSGL-1 molecules on the tethers and slings very similar to that obtained using the Alexa-Fluor-555-conjugated anti-PSGL-1 antibody (i.e. whole antibody with two binding sites) (Supplementary Note Fig. 1). This result demonstrates that the discrete spatial distribution of the PSGL-1 molecules on the tethers and slings are not the result of artificial clustering of PSGL-1 due to the bivalency effect of the antibody.

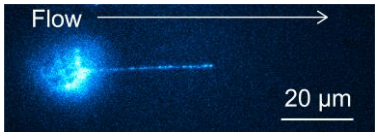

Supplementary Note Figure 1. Immunofluorescence image of PSGL-1 on KG1a cell captured using the Fab fragment of the anti-PSGL-1 antibody. The PSGL-1 molecules on the KG1a cells were immunostained by the Alexa-Fluor-555-conjugated Fab fragment of the anti-PSGL-1

antibody (KPL-1 clone). The fluorescence image was recorded during the KG1a cells rolling over E-selectin (15 molecules μm^{-2}) at a shear stress of 2 dyne cm^{-2}.

2. Density of CD44 on the tethers and slings

We calculated the number of the CD44 molecules per unit length of slings in a way similar to that for PSGL-1 (see Methods). The calculated densities of CD44 on the tethers and slings are in the range of 24 – 111 molecules μm^{-1} (i.e. the distances between adjacent CD44 molecules on the tethers and slings are in the range of 9 – 42 nm). This result demonstrates quantitatively that the densities of CD44 on the tethers and slings are much higher than those of PSGL-1 (0.4 – 0.8 μm distances between adjacent molecules on the tethers and slings, i.e. 1.25 – 2.5 molecules μm^{-1}). The distances between adjacent CD44 molecules on the tethers and slings estimated by the density calculation (9 – 42 nm) are much shorter than the spatial resolution of our fluorescence microscope (approximately 200 nm according to Rayleigh criterion). Therefore, individual CD44 molecules on the tethers and slings cannot be resolved in our fluorescence imaging experiment. This is consistent with the contiguous distribution of CD44 observed in our imaging experiment. The density of CD44 molecules on the tethers and slings decreased with an increase in the shear stress (Supplementary Note Fig. 2). Similar shear stress-dependent density was observed for PSGL-1 (Fig. 3g).

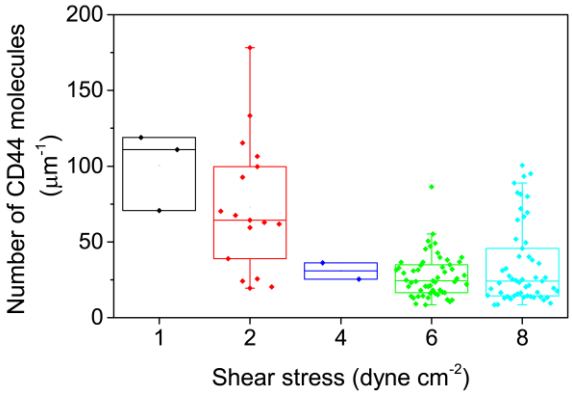

Supplementary Note Figure 2. Number of CD44 molecules per unit length of slings. The CD44 molecules on the KG1a cells were immunostained by the Alexa-Fluor-647-conjugated anti-CD44 antibody (515 clone). The fluorescence images were recorded during KG1a cell rolling over E-selectin (15 molecules μm^{-2}) at shear stresses of 1, 2, 4, 6 and 8 dynes cm^{-2}.

3. Comparison of E-selectin and P-selectin in terms of the tether formation

We observed the formation of the tethers with mean lengths of 18 – 30 μm at shear stresses ranging between 1 and 8 dyne cm^{-2} (Fig. 3f). Although the formation of tethers has been reported for neutrophils rolling over P-selectin(Sundd et al., 2012), relatively short tethers (mean lengths of approximately 10 μm) were observed only at high shear stresses (above 6 dyne cm^{-2})(Marki, Gutierrez, Mikulski, Groisman, & Ley, 2016). Although we cannot rule out the possibility that cell type dependent elastic properties of cell membranes may affect the tethering behaviour, it is more likely that the difference is due to the strength of selectin-ligand interactions. Our observations suggest that E-selectin-ligand interactions are much stronger than P-selectin-ligand interactions. Since rapture force of E-selectin-ligand interactions observed for polymorphonuclear leukocytes

is similar to that of P-selectin-ligand interactions(Hanley, Wirtz, & Konstantopoulos, 2004), it is likely that the difference in the binding strength between E-selectin and P-selectin is a result of different dissociation constants against their ligands. This is supported by our finding that KG1a cells roll faster over the P-selectin surfaces than E-selectin surfaces. The stronger binding (i.e. smaller dissociation rate) of the tethers resists shear stresses for longer periods of time before they dissociate from the surface selectins, and thus causes the formation of longer tethers. This stronger binding is consistent with previous studies from our lab illustrating that the k_{off} of binding between selectin ligands and E-selectin is low(AbuSamra et al., 2015; AbuSamra et al., 2017).

4. Elastic property of the tethers and slings and its contribution to cell rolling

The very bright and contiguous fluorescence of CD44 from the tethers and slings (Supplementary Fig. 11) allows detailed discussion about the dynamic behaviour of the tethers and slings. Our live-cell fluorescence imaging experiment clearly captured the flipping of the broken tethers from the rear side of the KG1a cell to its front side during rolling on E-selectin (Supplementary Fig. 11). The images demonstrate that the flipping of the tethers occurred at a time scale of approximately 240 ms. This time scale is longer than that reported for neutrophils rolling on P-selectin (less than 100 ms(Marki et al., 2016)), although similar tethers and slings were observed in both cell types. Given much larger shear stress (10 dyne cm^{-2}) used in the experiment on neutrophils compared with our experiment (Supplementary Fig. 11, 6 dyne cm^{-2}), the observed difference is likely to be due to the different flow velocities in these experiments rather than different elastic properties of the tethers formed in these experiments. These results indicate that the elastic properties of the

tethers and slings that make these structures so flexible are similar in different cell types, implying the existence of common mechanisms in the formation of tethers and slings.

5. Z-axis spatial resolution and cross-section ability of our 3D imaging system

We reconstructed 3D fluorescence images of CD44 and PSGL-1 on the rolling KG1a cells by recording epi-fluorescence images of the specimens at different Z-axis positions with 0.5 – 1.0 μm step size. Due to the fluorescence from out-of-focus regions, the reconstructed 3D fluorescence images of the cell body are distorted along the Z-axis and fine structures on the cell body cannot be resolved clearly. On the other hand, the width of the tethers and slings captured by the fluorescence images of CD44 and PSGL-1 is close to the diffraction-limited size defined by the Rayleigh criterion (0.21 – 0.33 μm in our experimental conditions). The depth of filed (Z) in our experimental conditions is calculated by using the following equation(Murphy & Davidson, 2012)

$$Z = \frac{n\lambda}{\mathrm{NA}^2} \quad ,$$

where n is the refractive index of the medium between the objective lens and the specimen. λ and NA denote the wavelength of light (i.e. fluorescence wavelength) and the numerical aperture of the objective lens. Given the optical characteristics of the objective lenses (n = 1.51, NA = 1.49 for UAPON 100XOTIRF and n = 1.41, NA = 1.25 for UPLSAPO40XS) and the spectroscopic properties of the fluorophores (λ = 0.5 – 0.67 μm) used in this study, the depth of field in our experiments is estimated to be in the range of 0.34 – 0.60 μm. Since the physical size (i.e. width and depth) of the tethers and slings is smaller than the depth of field, our imaging modes (i.e. capturing fluorescence images at different Z-axis positons with epi-illumination) enables to reconstruct the 3D image of the tethers and slings at the spatial resolution defined by the depth of field without the effect of out-of-focus fluorescence.

6. Shape of the frequency histograms of the number distribution of the PSGL-1 molecules

Frequency histograms of the number of the PSGL-1 molecules in each spot on the tethers and slings (Fig. 2b) can be fitted to Poisson distribution using the following equation

$$y = e^{-r}\frac{r^x}{x!},$$

where r is the mean of the distribution. This result indicates that the number of PSGL-1 molecules in each spot on the tethers and slings is determined in a stochastic way with the mean number of one PSGL-1 molecule per spot. Since the fluorescence labelling of the antibodies by the Alexa-Fluor-dyes also has as stochastic nature (i.e. each antibody carries a different number of the Alexa-Fluor-dyes whose distribution is described by Poisson distribution), the obtained Poisson distribution of the number of PSGL-1 molecules in each spot on the tethers and slings could be affected by this. However, the degree of labelling is in the range of 4 – 8 dyes per antibody, which should not give the experimentally observed Poisson distribution (i.e. mean number of one). Given the one-to-one binding of the antibody and PSGL-1, the result rather suggests that the number of PSGL-1 molecules in each spot on the tethers and slings is indeed determined in a stochastic way with the mean number of one PSGL-1 molecule per spot.

In contrast to the Poisson distributions obtained from the PSGL-1 molecules in each spot on the tethers and slings, frequency histograms of the number of the PSGL-1 molecules in each spot at the tethering points (Fig. 2c) and anchoring points (Fig. 2d) show a significant deviation from Poisson distribution. The result suggests that the number of PSGL-1 molecules in each tethering point and anchoring is not determined in a stochastic way. Instead, the result suggests the presence

of a mechanism that regulates the number of PSGL-1 in the tethering points. Given the larger number of the PSGL-1 molecules at the tethering points (on average 4.1 molecules) and anchoring points (on average 2.3 molecules), the mostly likely interpretation of the observation is that the formation of the tethering points and anchoring points is facilitated by the binding of multiple PSGL-1 molecules located in the close vicinity (i.e. spatially-clustered PSGL-1) to the surface E-selectin. The fact that larger numbers of the PSGL-1 molecules exist at the tethering points compared with those at anchoring points supports this interpretation. Since the anchoring points are formed after the initial tethering events occur, the tension exerted to the anchoring points should be smaller than that exerted to the tethering points. Thus, the smaller numbers of PSGL-1 at the anchoring points is an indication that the initial tether formation requires the binding of multiple PSGL-1 molecules to the surface E-selectins, which enables to resist high tension exerted to the tethering points. Note that we don't know yet if these anchoring points are formed at the rear side of the cells during the formation of the tethers. They may be formed during the sling binding to the surface at the front side of the cells as suggested by a previous study(Sundd et al., 2012).

7. Colocalisation of CD44 and membrane tethers/slings on MβCD-treated KG1a cells

The two-colour fluorescence imaging experiment of the membrane stain and CD44 on the control KG1a cells showed perfect spatial colocalisation of CD44 and the cell membrane in the tethers and slings (Fig. 1b, c), and thus the spatiotemporal behaviour of the tethers and slings (e.g. length of the tethers and slings at different applied shear stresses) can be characterized by analysing fluorescence images obtained for CD44. The MβCD treatment of the cells may alter the spatial

localisation of CD44, which may affect the analysis of the dynamic behaviour of the tethers and slings. We evaluated this by capturing two-colour fluorescence images of the membrane stain and CD44 on the MβCD-treated KG1a cells (Supplementary Note Fig. 3). While the tethers and slings of the MβCD-treated cells formed during cell rolling over E-selectin were much shorter than those of the control cells (Fig. 2i, k), we found perfect spatial colocalisation of the membrane stain and CD44 (Supplementary Note Fig. 3). This result confirms that the spatiotemporal behaviour of the tethers and slings on the MβCD-treated cells can be characterized by analysing fluorescence images obtained for CD44.

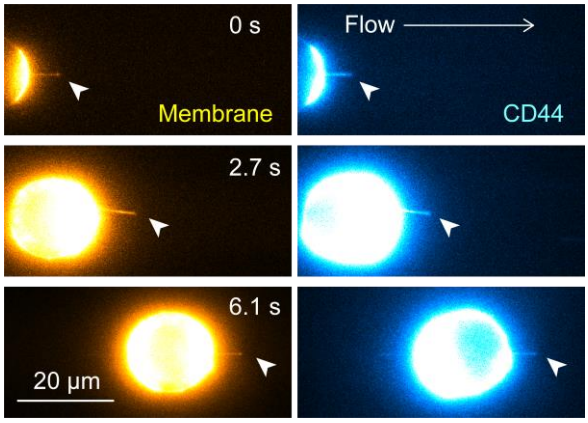

Supplementary Note Figure 3. Spatial colocalisation of CD44 and membrane tethers/slings on the MβCD-treated KG1a cells. Two-colour fluorescence images of the cell membrane (stained by Vybrant DiO dye) and CD44 (immunostained by Alexa-Fluor-647-conjugated anti-CD44 antibody clone 515) captured during the MβCD-treated KG1a cell rolling over the surface-deposited E-selectin molecules. White arrowheads show slings formed during the cell rolling. The stained and labelled cells were injected into the microfluidic chambers whose surface was coated

by rh E-selectin molecules at a density of 15 molecules μm^{-2}. The cells were injected into the chambers at a shear stress of 2 dyne cm^{-2}.

8. Localisations of PSGL-1 and CD44

We found that the PSGL-1 molecules show discrete distribution along the tethers and slings mostly as single molecules (Fig. 2b). Importantly, we observed larger numbers of PSGL-1 molecules at the tethering points (Fig. 2c) and the anchoring points (Fig. 2d). Although it is still controversial(Hocde, Hyrien, & Waugh, 2009; Snapp, Heitzig, & Kansas, 2002), PSGL-1 molecules are believed to localise to the tip of microvilli in order to facilitate efficient binding of PSGL-1 to selectins(Abbal et al., 2006; Miner et al., 2008; Moore et al., 1995). Previous work from our lab also suggested the localisation of CD44 to the microvilli of the cells(AbuZineh et al., 2018). Our findings in this study, in principle, agree with this model that the spatial confinement of the selectin ligands to microvilli enhances the probability that multiple ligand molecules in the confined area bind to P- or E-selectin on the surface, which leads to the formation of a tether against the tension exerted to the tethering point. Simulation studies suggested that spatial clustering of ligands strengthens ligand-receptor interactions(Gopalakrishnan, Forsten-Williams, Nugent, & Tauber, 2005) and helps cells to roll stably on a selectin surface(Schmidt, Papin, & Lawrence, 2009). While these studies did not consider the formation of the tethers and slings, the critical role of the spatial clustering of selectin ligands in the cell rolling reported in the study is consistent with our observation.

Previous studies suggested that PSGL-1 molecules localise to a tip of microvilli by their association with lipid rafts(Miner et al., 2008; B. J. Shao et al., 2015; Yago et al., 2010) and actin

binding proteins (ezrin/radixin/moesin (ERM) proteins)(Miner et al., 2008; Snapp et al., 2002). Our single-molecule imaging experiments revealed that PSGL-1 molecules distribute along the entire tethers and slings (Fig. 1f). This result suggests that these subcellular structures are disrupted during the formation of the tethers.

9. Effect of the retraction of the slings and rolling of the cells on the single-molecule diffusion analysis of PSGL-1

The single-molecule tracking analysis of the PSGL-1 molecules on the slings could be affected by the motion of the slings (i.e. either stable or retracting) and the cell (i.e. either rolling within the acquisition time of the diffusion trajectory or not). Thus, we split the diffusion trajectories into three categories and calculated the mean square displacement (MSD) versus time lag plots separately.

A. PSGL-1 molecules diffusing on the stable slings without the effect of the cell rolling.

B. PSGL-1 molecules diffusing on the retracting slings without the effect of the cell rolling.

C. PSGL-1 molecules diffusing on the stable slings with the effect of the cell rolling.

While we observed slight differences between the three cases, in principle, all the MSD versus time lag plots showed linear relationship (Supplementary Note Fig. 4). This result confirms the random-mode diffusion of the PSGL-1 molecules on the slings. The effect of the retraction of the slings and the cell rolling is negligible in our MSD analysis probably because of the decoupling of the time scale of the diffusional motion of the PSGL-1 molecules and the motion of the slings and the cells.

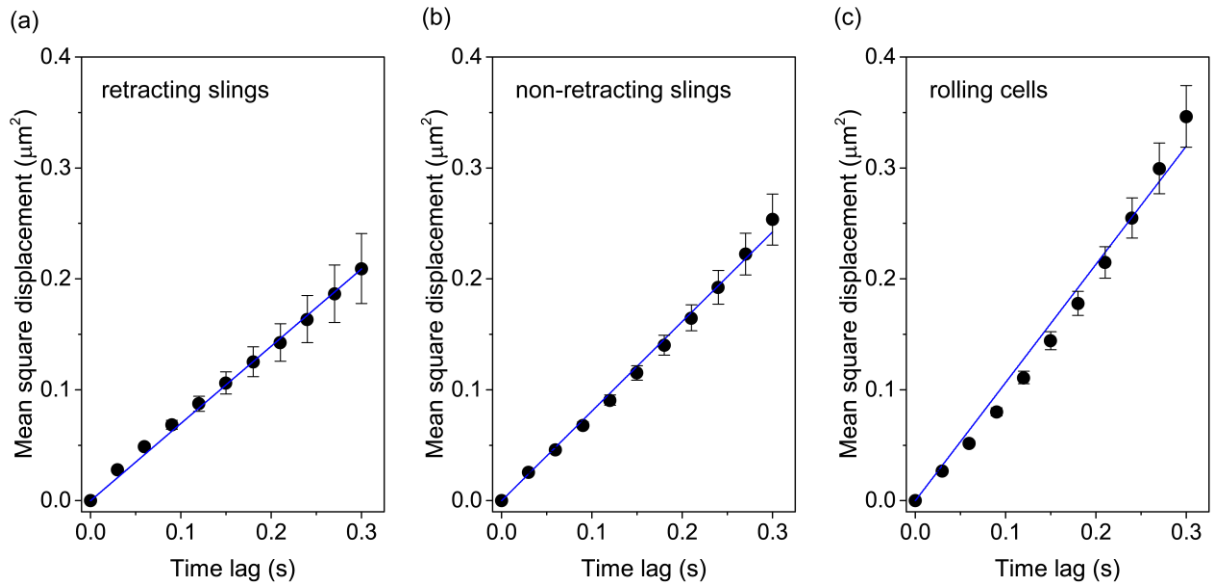

Supplementary Note Figure 4. MSD analysis of the PSGL-1 molecule diffusing on the slings. The MSD versus time lag plots were calculated using single-molecule diffusion trajectories of the PSGL-1 molecules diffusing on the (a) retracting slings without the effect of the cell rolling, (b) stable slings without the effect of the cell rolling and (c) stable slings with the effect of the cell rolling. The error bars show the standard errors of the mean determined by 47, 169 and 104 MSD plots obtained for the PSGL-1 molecules diffusing on the retracting slings, non-retracting slings and stable slings with the effect of the cell rolling, respectively.

10. Effect of the surface on the single-molecule tracking analysis and the interpretation of the obtained data

The single-molecule imaging experiment of the PSGL-1 molecules that are localised on the microvilli of the control KG1a cells (i.e. not rolling cells) was conducted by placing the immunostained cells on the surface of the microfluidic chamber. Although we did not deposit any

molecules that have a specific interaction with the PSGL-1 molecules (e.g. E-selectin), the PSGL-1 molecule may interact with the surface in a nonspecific manner, and therefore the diffusional motion of the PSGL-1 may be affected. We investigated this effect by analysing the single-molecule diffusion trajectories obtained from both the bottom and top surfaces of the cells. To minimize the effect of the refractive index mismatch between the cell samples and the immersion media, we used the silicone immersion objective lens (60× NA = 1.3, UPLSAPO60XS2) for this imaging experiment. The MSD versus time lag plots obtained from these experiments showed very similar behaviour, including smaller diffusion coefficient compared with that obtained from the PSGL-1 molecules on the tethers and slings and confined-mode diffusion (Supplementary Note Fig. 5a). Quantitative analysis of the MSD versus time lag plots revealed that the PSGL-1 molecules localised on the microvilli at both the bottom and top surface of the cells show similar diffusion coefficient and the confined size (Supplementary Note Fig. 5b, c). These results confirm that there is a negligible effect of the surface on the diffusional motion of the PSGL-1 molecules localised on microvilli. We used the data obtained from the bottom surface of the cells for the analysis as we obtained slightly better quality of the single-molecule fluorescence images of the PSGL-1 molecules from the bottom surface of the cells.

The diffusion coefficient of the PSGL-1 molecules localised on the microvilli of the control KG1a cells obtained from the MSD analysis (0.1 $\mu m^2\ s^{-1}$) is approximately 30 fold larger than the diffusion coefficient of PSGL-1 reported previously using fluorescence recovery after photobleaching (FRAP) technique (0.003 $\mu m^2\ s^{-1}$)(Gaborski, Clark, Waugh, & McGrath, 2008). Given the different time and length scales of the diffusional motion captured by these two methods, it is very likely that we captured the motion of microvilli rather than the diffusional motion of the PSGL-1 molecules in our single-molecule fluorescence imaging experiment (i.e. the PSGL-1

molecules stay at the tip of microvilli during the image acquisition and therefore we capture the motion of the microvilli through the fluorescence signal of the PSGL-1 molecules). This is strongly supported by the fact that the size of the confinement area (0.29 μm^2 that corresponds to the confinement length of approximately 0.54 μm) estimated by the MSD analysis is close to the size of the area expected to be covered by the microvilli since our SEM experiments on the KG1a cells revealed that the length of the microvilli is in the range of several hundred of nanometres (Fig. 2g). Also, the length of the microvilli on neutrophils has been estimated to be about 0.3 μm(J. Y. Shao, Ting-Beall, & Hochmuth, 1998). Therefore, the real diffusion coefficient of the PSGL-1 molecules localised on the microvilli would be much smaller than our estimation by the MSD analysis of the single-molecule diffusion trajectories and may be closer to the value determined by the FRAP technique. The difference in the diffusion coefficient obtained in our experiment and in the previous study may also be partly explained by differences from cell to cell.

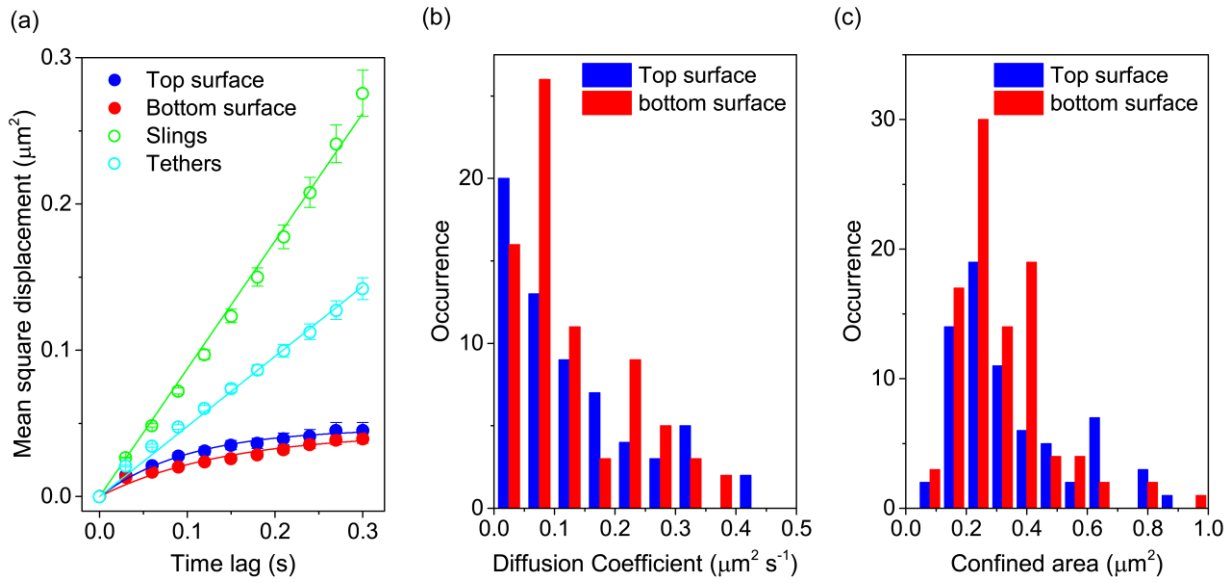

Supplementary Note Figure 5. MSD analysis of the PSGL-1 molecule localised on the microvilli. (a) MSD versus time lag plots calculated using single-molecule diffusion trajectories of the PSGL-1 molecules localised on the microvilli of the control KG1a cells at the top (blue) and bottom (red) surface of the cells. The error bars show the standard errors of the mean determined by 126 and 129 MSD plots obtained for the PSGL-1 molecules localised on the microvilli of the control KG1a cells at the top and bottom surface of the cells. The MSD versus time lag plots obtained from the single-molecule diffusion trajectories of the PSGL-1 molecules diffusing on the tethers (cyan) and slings (green) are also displayed as a comparison. Frequency histograms of the (b) diffusion coefficient and (c) confined area of the PSGL-1 molecules on the microvilli of the control KG1a cells at the top (blue) and bottom (red) surface of the cells.

Captions for Supplementary Video 1 to 7

Supplementary Movie 1: Time-lapse fluorescence images of CD44 on a KG1a cell perfused into a microfluidic chamber at a shear stress of 1 – 8 dyne cm^{-2}. The CD44 molecules were immunostained by Alexa-Fluor-647-conjugated anti-CD44 antibody, clone 515. The surface of the microfluidic chamber was coated with rh E-selectin molecules at a density of 15 molecules μm^{-2}. Scale bar = 20 μm.

Supplementary Movie 2: Time-lapse fluorescence images of CD44 on a KG1a cell perfused into a microfluidic chamber that shows the conversion of a tether into sling. The CD44 molecules were immunostained by Alexa-Fluor-647-conjugated anti-CD44 antibody, clone 515. The cells were injected into the chambers at a shear stress of 6 dyne cm^{-2}. The surface of the microfluidic chamber was coated with rh E-selectin molecules at a density of 15 molecules μm^{-2}. Scale bar = 20 μm.

Supplementary Movie 3: Time-lapse fluorescence images of CD44 on a KG1a cell perfused into a microfluidic chamber that shows the retraction of the sling. The CD44 molecules were immunostained by Alexa-Fluor-647-conjugated anti-CD44 antibody, clone 515. The cells were injected into the chambers at a shear stress of 8 dyne cm^{-2}. The surface of the microfluidic chamber was coated with rh E-selectin molecules at a density of 15 molecules μm^{-2}. Scale bar = 20 μm.

Supplementary Movie 4: Time-lapse fluorescence images of PSGL-1 on a KG1a cell perfused into a microfluidic chamber that shows the discrete spatial distribution of the PSGL-1 molecules on the tether. The PSGL- molecules were immunostained by Alexa-Fluor-555-conjugated anti-PSGL-1 antibody, clone KPL-1. The cells were injected into the chambers at the

shear stress of 2 dyne cm^{-2}. The surface of the microfluidic chamber was coated with rh E-selectin molecules at a density of 15 molecules μm^{-2}. Scale bar = 10 μm.

Supplementary Movie 5: Time-lapse fluorescence images of PSGL-1 on a KG1a cell perfused into a microfluidic chamber that shows the discrete spatial distribution of the PSGL-1 molecules on the sling. The PSGL- molecules were immunostained by Alexa-Fluor-555-conjugated anti-PSGL-1 antibody, clone KPL-1. The cells were injected into the chambers at a shear stress of 2 dyne cm^{-2}. The surface of the microfluidic chamber was coated with rh E-selectin molecules at a density of 15 molecules μm^{-2}. Scale bar = 10 μm.

Supplementary Movie 6: Time-lapse fluorescence images of CD44 on KG1a cells perfused into a microfluidic chamber that shows the formation of the tethers and slings on all the rolling cells. The CD44 molecules were immunostained by Alexa-Fluor-647-conjugated anti-CD44 antibody, clone 515. The cells were injected into the chambers at a shear stress of 4 dyne cm^{-2}. The surface of the microfluidic chamber was coated with rh E-selectin molecules at a density of 15 molecules μm^{-2}. Scale bar = 20 μm.

Supplementary Movie 7: Time-lapse fluorescence images of PSGL-1 on a KG1a cell perfused into a microfluidic chamber that shows the merger of multiple tethers. The PSGL- molecules were immunostained by Alexa-Fluor-555-conjugated anti-PSGL-1 antibody, clone KPL-1. The cells were injected into the chambers at a shear stress of 2 dyne cm^{-2}. The surface of the microfluidic chamber was coated with rh E-selectin molecules at a density of 15 molecules μm^{-2}. Scale bar = 5 μm.

Supplementary References

Abbal, C., Lambelet, M., Bertaggia, D., Gerbex, C., Martinez, M., Arcaro, A., . . . Spertini, O. (2006). Lipid raft adhesion receptors and Syk regulate selectin-dependent rolling under flow conditions. *Blood, 108*(10), 3352-3359. doi:10.1182/blood-2006-04-013912

AbuSamra, D. B., Al-Kilani, A., Hamdan, S. M., Sakashita, K., Gadhoum, S. Z., & Merzaban, J. S. (2015). Quantitative characterization of E-selectin interaction with native CD44 and P-selectin glycoprotein ligand-1 (PSGL-1) using a real time immunoprecipitation-based binding assay. *Journal of Biological Chemistry, 290*(35), 21213-21230. doi:10.1074/jbc.M114.629451

AbuSamra, D. B., Aleisa, F. A., Al-Amoodi, A. S., Jalal Ahmed, H. M., Chin, C. J., Abuelela, A. F., . . . Merzaban, J. S. (2017). Not just a marker: CD34 on human hematopoietic stem/progenitor cells dominates vascular selectin binding along with CD44. *Blood Adv, 1*(27), 2799-2816. doi:10.1182/bloodadvances.2017004317

AbuZineh, K., Joudeh, L. I., Al Alwan, B., Hamdan, S. M., Merzaban, J. S., & Habuchi, S. (2018). Microfluidics-based super-resolution microscopy enables nanoscopic characterization of blood stem cell rolling. *Science Advances, 4*(7), eaat5304. doi:10.1126/sciadv.aat5304

Gaborski, T. R., Clark, A., Waugh, R. E., & McGrath, J. L. (2008). Membrane Mobility of beta 2 Integrins and Rolling Associated Adhesion Molecules in Resting Neutrophils. *Biophysical Journal, 95*(10), 4934-4947. doi:10.1529/biophysj.108.132886

Gopalakrishnan, M., Forsten-Williams, K., Nugent, M. A., & Tauber, U. C. (2005). Effects of receptor clustering on ligand dissociation kinetics: Theory and simulations. *Biophysical Journal, 89*(6), 3686-3700. doi:10.1529/biophysj.105.065300

Hanley, W. D., Wirtz, D., & Konstantopoulos, K. (2004). Distinct kinetic and mechanical properties govern selectin-leukocyte interactions. *Journal of Cell Science, 117*(12), 2503-2511. doi:10.1242/jcs.01088

Hocde, S. A., Hyrien, O., & Waugh, R. E. (2009). Cell Adhesion Molecule Distribution Relative to Neutrophil Surface Topography Assessed by TIRFM. *Biophysical Journal, 97*(1), 379-387. doi:10.1016/j.bpj.2009.04.035

Marki, A., Gutierrez, E., Mikulski, Z., Groisman, A., & Ley, K. (2016). Microfluidics-based side view flow chamber reveals tether-to-sling transition in rolling neutrophils. *Scientific Reports, 6*, 8. doi:10.1038/srep28870

Miner, J. J., Xia, L., Yago, T., Kappelmayer, J., Liu, Z., Klopocki, A. G., . . . McEver, R. P. (2008). Separable requirements for cytoplasmic domain of PSGL-1 in leukocyte rolling and signaling under flow. *Blood, 112*(5), 2035-2045. doi:10.1182/blood-2008-04-149468

Moore, K. L., Patel, K. D., Bruehl, R. E., Li, F. G., Johnson, D. A., Lichenstein, H. S., . . . McEver, R. P. (1995). P-selectin glycoprotein ligand-1 mediates rolling of human neutrophils on P-selectin. *Journal of Cell Biology, 128*(4), 661-671. doi:10.1083/jcb.128.4.661

Murphy, D. B., & Davidson, M. W. (2012). *Fundamental of light microscopy and electronic imaging*: Wiley-Blackwell.

Schmidt, B. J., Papin, J. A., & Lawrence, M. B. (2009). Nano-motion Dynamics are Determined by Surface-Tethered Selectin Mechanokinetics and Bond Formation. *Plos Computational Biology, 5*(12), 19. doi:10.1371/journal.pcbi.1000612

Shao, B. J., Yago, T., Setiadi, H., Wang, Y., Mehta-D'souza, P., Fu, J. X., . . . McEver, R. P. (2015). O-glycans direct selectin ligands to lipid rafts on leukocytes. *Proceedings of the National Academy of Sciences of the United States of America, 112*(28), 8661-8666. doi:10.1073/pnas.1507712112

Shao, J. Y., Ting-Beall, H. P., & Hochmuth, R. M. (1998). Static and dynamic lengths of neutrophil microvilli. *Proceedings of the National Academy of Sciences of the United States of America, 95*(12), 6797-6802. doi:10.1073/pnas.95.12.6797

Snapp, K. R., Heitzig, C. E., & Kansas, G. S. (2002). Attachment of the PSGL-1 cytoplasmic domain to the actin cytoskeleton is essential for leukocyte rolling on P-selectin. *Blood, 99*(12), 4494-4502. doi:10.1182/blood.V99.12.4494

Sundd, P., Gutierrez, E., Koltsova, E. K., Kuwano, Y., Fukuda, S., Pospieszalska, M. K., . . . Ley, K. (2012). 'Slings' enable neutrophil rolling at high shear. *Nature, 488*(7411), 399-403. doi:10.1038/nature11248

Yago, T., Shao, B. J., Miner, J. J., Yao, L. B., Klopocki, A. G., Maeda, K., . . . McEver, R. P. (2010). E-selectin engages PSGL-1 and CD44 through a common signaling pathway to induce integrin alpha(L)beta(2)-mediated slow leukocyte rolling. *Blood, 116*(3), 485-494. doi:10.1182/blood-2009-12-259556